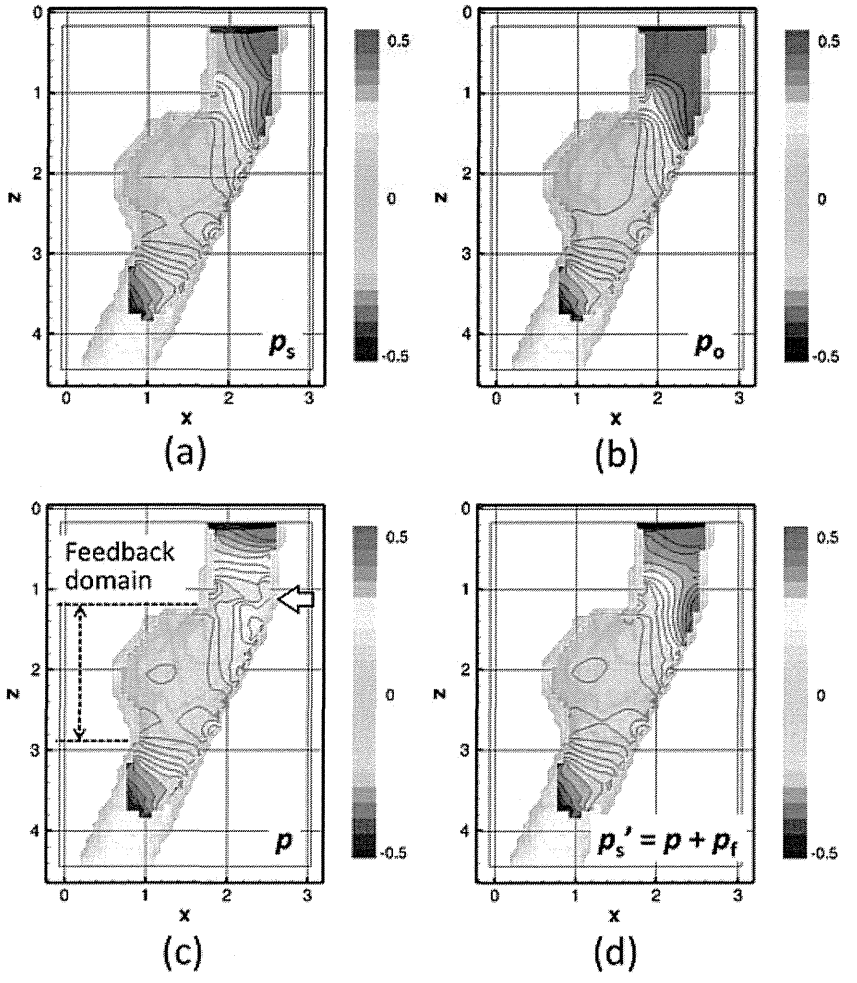

Figure 6. Pressure distribution on a y-directional cross-section ($y = 1.462$): (a) standard solution, p_s, (b) ordinary simulation $\left(K_v^* = 0\right)$, p_o, and UMI simulations (c) without and (d) with pressure compensation at $K_v^* = 160$, p and p_s', respectively (nondimensional).

boundary and in the vicinity of the upstream boundary of the feedback domain, respectively. In contrast, the error in the UMI simulation with the pressure compensation is relatively small in the whole domain.

The distribution of the divergence of the feedback force vector in the UMI simulation is demonstrated in Figure 8(a). There is a region with a large magnitude of divergence of the feedback force vector near the upstream boundary of the feedback domain. Figure 8(b) shows the distribution of the pressure compensation in the UMI simulation, p_f, calculated from Equation (9). It is noted that the distribution of the pressure compensation has a pattern similar to that of the error norm of the pressure for the UMI simulation without the pressure compensation in Figure 7(b). By adding the pressure compensation, p_f (Figure 8(b)), to the result of the UMI simulation without compensation (Figure 6(c)), a compensated pressure field, p_s' (Figure 6(d)), is obtained.

In summary, the numerical experiment dealing with a three-dimensional steady flow in a thoracic aneurysm indicates that feedback signals in the UMI simulation can deteriorate the reproducibility of the pressure field, while improving that of the velocity field. However, by properly compensating the effects of the feedback signals on the pressure with the proposed method, both the velocity and pressure fields of the standard solution can be properly reproduced.

DOI: 10.1002/cnm

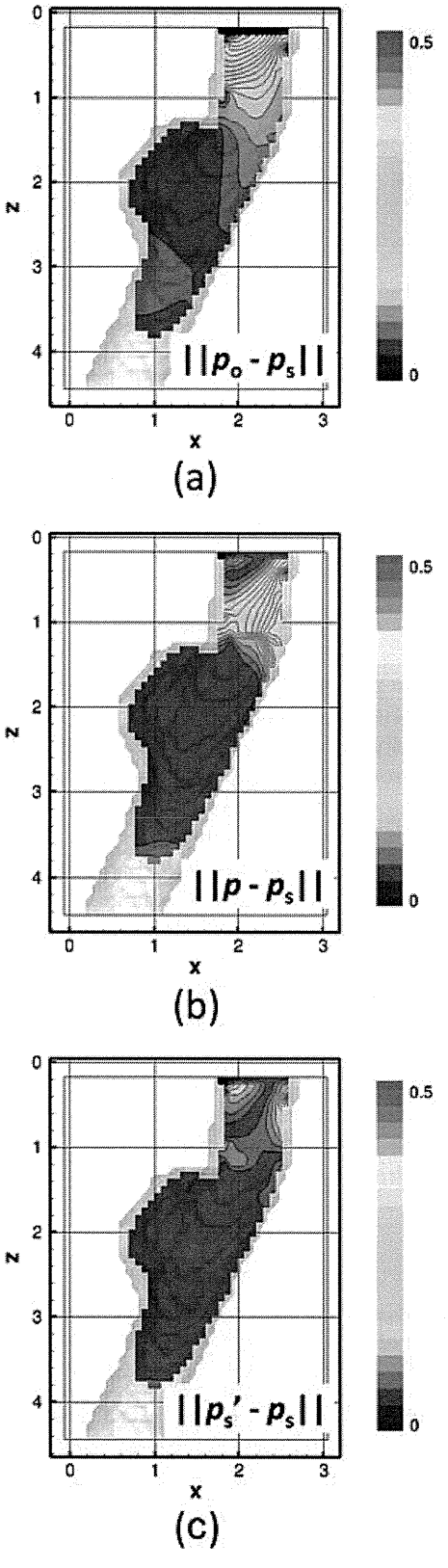

Figure 7. Error norm of pressure on a y-directional cross-section ($y = 1.462$): (a) ordinary numerical simulation $\left(K_v^* = 0\right)$, and UMI simulations (b) without and (c) with pressure compensation at $K_v^* = 160$, respectively (nondimensional).

DOI: 10.1002/cnm

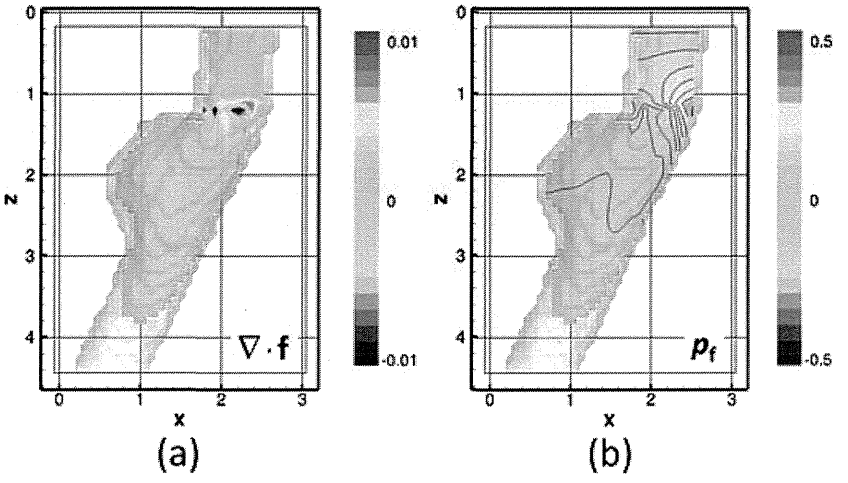

Figure 8. Distributions of (a) divergence of feedback force vector and (b) value for pressure compensation, p_f, in the UMI simulation at $K_v^* = 160$ (nondimensional).

4. CONCLUSION

In this study, reproduction of the pressure field by UMI simulation was investigated. The effect of feedback based on Doppler velocity on the pressure field was first examined by theoretical analysis. When the divergence of the feedback force vector was not zero, it influenced the pressure field in the UMI simulation, while improving the computational accuracy of the velocity field. Hence, a method to estimate the correct pressure by compensating the pressure field was devised. A numerical experiment was conducted dealing with the reproduction of a three-dimensional steady flow in a thoracic aneurysm to validate results of the theoretical analysis. The ability of the UMI simulation to reproduce the pressure field deteriorated with a large feedback gain. However, by properly compensating the effects of the feedback signals on the pressure, the error in the pressure field was reduced, exhibiting improvement of the computational accuracy in comparison with that of the ordinary simulation. Hence, the UMI simulation with pressure compensation allows for the reproduction of both velocity and pressure fields of blood flow. The information on hemodynamic stresses (wall shear stress and pressure) and blood flow dynamics enables a better understanding of blood flow and would provide novel indices for diagnosis of diseases. To perform the UMI simulation in a clinical setting, further investigations on automatic excursion of the sequential computation including reconstruction of the blood vessel configuration and recognitions of the position and orientation of the ultrasound probe are required.

REFERENCES

1. Friedman MH, Krams R, Chandran KB. Flow interactions with cells and tissues: cardiovascular flows and fluid-structure interactions. *Annals of Biomedical Engineering* 2010; **38**:1178–1187.
2. Taylor CA, Steinman DA. Image-based modeling of blood flow and vessel wall dynamics: applications, methods and future directions. *Annals of Biomedical Engineering* 2010; **38**:1188–1203.
3. Morris L, Delassus P, Grace P, Wallis F, Walsh M, McGloughlin T. Effects of flat, parabolic and realistic steady flow inlet profiles on idealised and realistic stent graft fits through Abdominal Aortic Aneurysms (AAA). *Medical Engineering & Physics* 2006; **28**:19–26.
4. Moyle KR, Antiga L, Steinman DA. Inlet conditions for image-based CFD models of the carotid bifurcation: is it reasonable to assume fully developed flow? *Journal of Biomechanical Engineering-Transactions of the ASME* 2006; **128**:371–379.
5. Formaggia L, Gerbeau JF, Nobile F, Quarteroni A. Numerical treatment of defective boundary conditions for the Navier-Stokes equations. *SIAM Journal on Numerical Analysis* 2002; **40**:376–401.
6. Veneziani A, Vergara C. An approximate method for solving incompressible Navier-Stokes problems with flow rate conditions. *Computer Methods in Applied Mechanics and Engineering* 2007; **196**:1685–1700.

7. McGregor RH, Szczerba D, von Siebenthal M, Muralidhar K, Szekely G. Exploring the use of proper orthogonal decomposition for enhancing blood flow images via computational fluid dynamics. *Medical Image Computing and Computer Assisted Intervention* 2008; **11**:782–789.
8. McGregor RH, Szczerbal D, Muralidhar K, Szekely G. A fast alternative to computational fluid dynamics for high quality imaging of blood flow. *Medical Image Computing and Computer Assisted Intervention* 2009; **12**:124–131.
9. Zeldin BA, Meade AJ. Integrating experimental data and mathematical models in simulation of physical systems. *AIAA Journal* 1997; **35**:1787–1790.
10. Dwight RP. Bayesian inference for data assimilation using least-squares finite element methods. *IOP Conference Series: Materials Science and Engineering* 2010; **10**:012224.
11. Heys JJ, Manteuffel TA, McCormick SF, Milano M, Westerdale J, Belohlavek M. Weighted least-squares finite elements based on particle imaging velocimetry data. *Journal of Computational Physics* 2010; **229**:107–118.
12. Bertoglio C, Moireau P, Gerbeau JF. Sequential parameter estimation for fluid-structure problems. Application to hemodynamics. *International Journal for Numerical Methods in Biomedical Engineering* 2012; **28**:434–455.
13. D'Elia M, Perego M, Veneziani A. A variational data assimilation procedure for the incompressible Navier-Stokes equations in hemodynamics. *Journal of Scientific Computing* 2012; **52**:340–359.
14. Munro R, Kopken C, Kelly G, Thepaut JN, Saunders R. Assimilation of Meteosat radiance data within the 4D-Var system at ECMWF: data quality monitoring, bias correction and single-cycle experiments. *Quarterly Journal of the Royal Meteorological Society* 2004; **130**:2293–2313.
15. Hayase T, Hayashi S. State estimator of flow as an integrated computational method with the feedback of online experimental measurement. *Journal of Fluids Engineering-Transactions of the ASME* 1997; **119**:814–822.
16. Nisugi K, Hayase T, Shirai A. Fundamental study of hybrid wind tunnel integrating numerical simulation and experiment in analysis of flow field. *JSME International Journal Series B-Fluids and Thermal Engineering* 2004; **47**:593–604.
17. Yamagata T, Hayase T, Higuchi H. Effect of feedback data rate in PIV measurement-integrated simulation. *Journal of Fluid Science and Technology* 2008; **3**:477–487.
18. Nakao M, Kawashima K, Kagawa T. Application of MI simulation using a turbulent model for unsteady orifice flow. *Journal of Fluids Engineering-Transactions of the ASME* 2009; **131**:111401.
19. Funamoto K, Hayase T, Shirai A, Saijo Y, Yambe T. Fundamental study of ultrasonic-measurement-integrated simulation of real blood flow in the aorta. *Annals of Biomedical Engineering* 2005; **33**:415–428.
20. Funamoto K, Suzuki Y, Hayase T, Kosugi T, Isoda H. Numerical validation of MR-measurement-integrated simulation of blood flow in a cerebral aneurysm. *Annals of Biomedical Engineering* 2009; **37**:1105–1116.
21. Funamoto K, Hayase T, Saijo Y, Yambe T. Numerical experiment for ultrasonic-measurement-integrated simulation of three-dimensional unsteady blood flow. *Annals of Biomedical Engineering* 2008; **36**:1383–1397.
22. Funamoto K, Hayase T, Saijo Y, Yambe T. Numerical experiment of transient and steady characteristics of ultrasonic-measurement-integrated simulation in three-dimensional blood flow analysis. *Annals of Biomedical Engineering* 2009; **37**:34–49.
23. Funamoto K, Hayase T, Saijo Y, Yambe T. Numerical analysis of effects of measurement errors on ultrasonic-measurement-integrated simulation. *IEEE Transactions on Biomedical Engineering* 2011; **58**:653–663.
24. Funamoto K, Hayase T, Saijo Y, Yambe T. Numerical study on variation of feedback methods in ultrasonic-measurement-integrated simulation of blood flow in the aneurysmal aorta. *JSME International Journal Series C-Mechanical Systems, Machine Elements and Manufacturing* 2006; **49**:144–155.
25. Arfken GB, Weber HJ. *Mathematical Methods for Physicists*. Elsevier Academic Press: Amsterdam/Boston/Tokyo, 2005.
26. Patankar SV. *Numerical Heat Transfer and Fluid Flow*. Hemisphere Pub. Corp.: Washington DC/New York, 1980.
27. Morbiducci U, Ponzini R, Rizzo G, Biancolini ME, Iannaccone F, Gallo D, Redaelli A. Synthetic dataset generation for the analysis and the evaluation of image-based hemodynamics of the human aorta. *Medical & Biological Engineering & Computing* 2012; **50**:145–154.
28. Swillens A, De Schryver T, Lovstakken L, Torp H, Segers P. Assessment of numerical simulation strategies for ultrasonic color blood flow imaging, based on a computer and experimental model of the carotid artery. *Annals of Biomedical Engineering* 2009; **37**:2188–2199.
29. Hayase T, Humphrey JAC, Greif R. Mini-manual for ROTFLO2. *Department of Mechanical Engineering Report*, University of California, Berkeley, 1990; FM-90-1.
30. Hayase T, Humphrey JAC, Greif R. A consistently formulated QUICK scheme for fast and stable convergence using finite-volume iterative calculation procedures. *Journal of Computational Physics* 1992; **98**:108–118.
31. Schneider GE, Zedan M. A modified strongly implicit procedure for the numerical solution of field problems. *Numerical Heat Transfer* 1981; **4**:1–19.
32. Hayase T, Imagawa K, Funamoto K, Shirai A. Stabilization of measurement-integrated simulation by elucidation of destabilizing mechanism. *Journal of Fluid Science and Technology* 2010; **5**:632–647.

DOI: 10.1002/cnm

Novel ^{18}F-Labeled Arylquinoline Derivatives for Noninvasive Imaging of Tau Pathology in Alzheimer Disease

Nobuyuki Okamura[1], Shozo Furumoto[1,2], Ryuichi Harada[1], Tetsuro Tago[2], Takeo Yoshikawa[1], Michelle Fodero-Tavoletti[3], Rachel S. Mulligan[4], Victor L. Villemagne[4], Hiroyasu Akatsu[5], Takayuki Yamamoto[5], Hiroyuki Arai[6], Ren Iwata[2], Kazuhiko Yanai[1], and Yukitsuka Kudo[7]

[1]Department of Pharmacology, Tohoku University School of Medicine, Sendai, Japan; [2]Division of Radiopharmaceutical Chemistry, Cyclotron and Radioisotope Center, Tohoku University, Sendai, Japan; [3]Department of Pathology, University of Melbourne, Victoria, Australia; [4]Department of Nuclear Medicine and Centre for PET, Austin Health, Melbourne, Victoria, Australia; [5]Choju Medical Institute, Fukushimura Hospital, Toyohashi, Japan; [6]Department of Geriatrics and Gerontology, Institute of Development, Aging and Cancer, Tohoku University, Sendai, Japan; and [7]Clinical Research, Innovation and Education Center, Tohoku University Hospital, Sendai, Japan

Neurofibrillary tangles in Alzheimer disease (AD) brains are composed of the microtubule-associated protein tau. Noninvasive monitoring of tau protein aggregates in the living brain will provide useful information regarding tau pathophysiology in AD. However, no PET probes are currently available for selective detection of tau pathology in AD. We have previously reported ^{18}F-labeled THK-523 (^{18}F-6-(2-fluoroethoxy)-2-(4-aminophenyl)quinoline) as a tau imaging radiotracer candidate for PET. After compound optimization, we developed novel ^{18}F-labeled arylquinoline derivatives, ^{18}F-THK-5105 and ^{18}F-THK-5117, for use as tau imaging PET tracers. **Methods:** ^{18}F-labeled compounds were prepared from the corresponding tosylated precursors. The binding affinity of compounds to synthetic tau aggregates and tau-rich AD brain homogenates was determined by saturation and competition binding assays. The binding selectivity of compounds to tau pathology was evaluated by autoradiography of AD brain sections. The pharmacokinetics of compounds were assessed in biodistribution studies in normal mice. A 14-d toxicity study with intravenous administration of compounds was performed using rats and mice. **Results:** In vitro binding assays demonstrated higher binding affinity of THK-5105 and THK-5117 than THK-523 to tau protein aggregates and tau-rich AD brain homogenates. Autoradiographic analyses of AD brain sections showed that these radiotracers preferentially bound to neurofibrillary tangles and neuropil threads, which colocalized with Gallyas-positive and immunoreactive tau protein deposits. The distribution of this radiotracer binding in AD brain sections was completely different from that of ^{11}C-Pittsburgh compound B, showing preferential binding to amyloid plaques. Furthermore, these derivatives demonstrated abundant initial brain uptake and faster clearance in normal mice than ^{18}F-THK-523 and other reported ^{18}F-labeled radiotracers. THK-5105 and THK-5117 showed no toxic effects related to the administration of these compounds in mice and rats and no significant binding for various neuroreceptors, ion channels, and transporters at 1-μM concentrations. **Conclusion:** ^{18}F-labeled THK-5105 and THK-5117 are promising candidates as PET tau imaging radiotracers.

Received Nov. 19, 2012; revision accepted Feb. 19, 2013.
For correspondence or reprints contact: Nobuyuki Okamura, 2-1, Seiryo-machi, Aoba-ku, Sendai 980-8575 Japan.
E-mail: nookamura@med.tohoku.ac.jp
Published online Jul. 15, 2013.

Key Words: Alzheimer disease; tau; neurofibrillary tangles; positron emission tomography; molecular imaging

J Nucl Med 2013; 54:1420–1427
DOI: 10.2967/jnumed.112.117341

Alzheimer disease (AD) is the most common cause of dementia in the elderly. At present, approximately 18 million people worldwide have AD, and this number is estimated to double by 2025 (*1*). The major pathologic hallmarks of AD are senile plaques (SPs) and neurofibrillary tangles (NFTs). SPs are composed of amyloid-β protein (Aβ), a 39–43 amino acid protein product derived from the proteolytic cleavage of the amyloid precursor protein. Abnormalities in the production or clearance of Aβ are considered to be the initiating events in AD pathogenesis (*2*). Excessive Aβ concentrations lead to its aggregation and formation of SPs, followed by NFT formations, synaptic dysfunction, and neuronal death. NFTs are composed of hyperphosphorylated tau, a microtubule-associated protein that stabilizes microtubule assembly in axons (*3*). Tau accumulation is also recognized as neuropil threads and dystrophic neurites in the AD brain (*4*). Phosphorylation of tau decreases its ability to bind to microtubules, which are destabilized, leading to neuronal death. NFT lesions follow a stereotypical pattern, initially appearing in the transentorhinal cortex, followed by the entorhinal cortex and the hippocampus, and subsequently the neocortex (*5*). In AD patients, the severity of tau pathology is closely related to neuronal loss (*6,7*) and cognitive impairment (*8,9*). The deposition of NFTs is thought to begin before extensive neuronal loss and cognitive decline occur. Thus, noninvasive detection of tau pathology would be useful to predict future cognitive decline in the preclinical stages of AD and to track disease progression before extensive neuronal loss occurs.

Several researchers have focused on developing radiotracers for imaging tau pathology in the human brain (*10–17*). Tau imaging radiotracers need to cross the blood–brain barrier and to have a high binding affinity to NFTs with minimal nonspecific binding (*18*). 2-(1-(6-[(2-^{18}F-fluoroethyl)(methyl)amino]-2-naphthyl)ethylidene)malononitrile (^{18}F-FDDNP) is claimed as the only PET tracer that allows measurement of the amount of tau protein

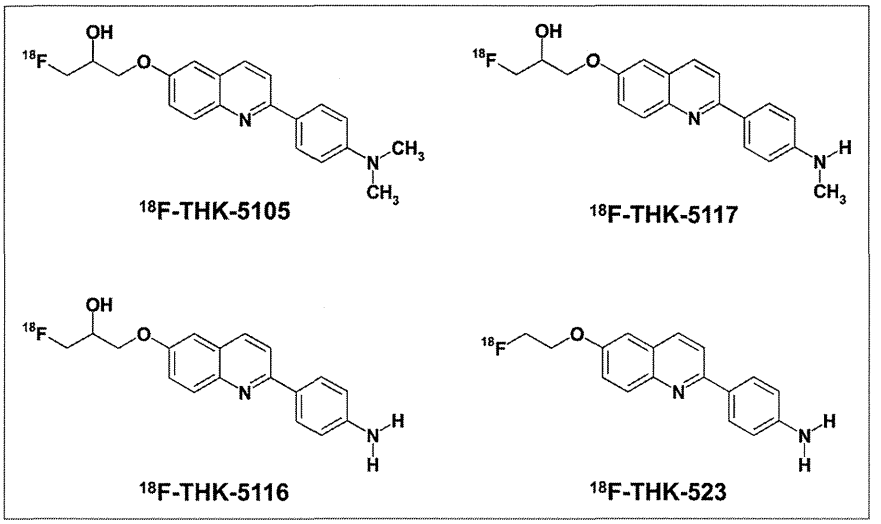

FIGURE 1. Chemical structures of ^{18}F-THK-5105, ^{18}F-THK-5116, ^{18}F-THK-5117, and ^{18}F-THK-523.

deposits in the human brain (*19*). However, ^{18}F-FDDNP was found to have lower binding affinity for protein fibrils than ^{11}C-Pittsburgh compound B (^{11}C-PiB) (*20,21*). In addition, this tracer has been claimed to bind to both SPs and NFTs equally (*22*). In the neocortex of the AD brain, SPs and NFTs colocalize with each other, where Aβ concentrations are 5–20 times higher than that of tau (*23,24*). In such cases, the signal from the SPs would be so overwhelming that it would obscure the signal from the NFTs. Therefore, the development of selective tau imaging tracers is necessary for accurate and quantitative evaluation of tau pathology in AD.

In the past few years, we also have screened more than 2,000 compounds to develop novel radiotracers with high affinity and selectivity for tau aggregates. Consequently, we identified a series of novel quinoline and benzimidazole derivatives that bind NFTs and, to a lesser extent, Aβ plaques (*10*). Serial analyses of these compounds led to the design and synthesis of the novel tau imaging agent ^{18}F-6-(2-fluoroethoxy)-2-(4-aminophenyl)quinoline (^{18}F-THK-523) (*15,17*). Preclinical analyses of ^{18}F-THK-523 indicated that this tracer selectively labels tau pathology in the AD brain. However, the preclinical data suggest that the pharmacokinetics and binding characteristics of ^{18}F-THK-523 might not reach the necessary optimal levels required for PET tracers. Through our optimization process, we developed novel ^{18}F-labeled 2-arylquinoline derivatives that are promising candidates for in vivo tau imaging probes. In this study, we performed the preclinical evaluation of the binding and pharmacokinetic properties of these compounds.

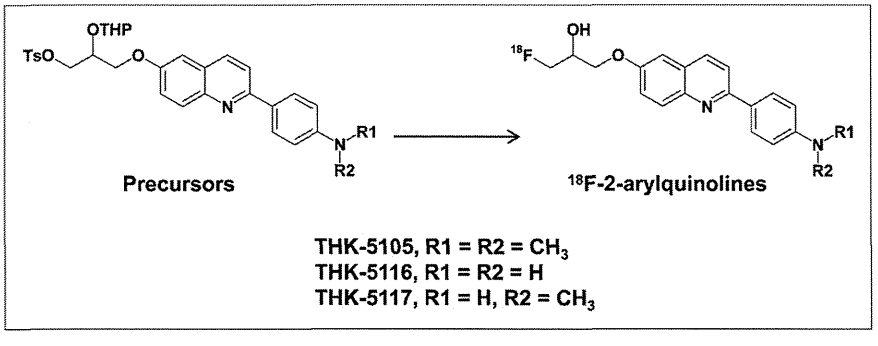

FIGURE 2. Radiosynthesis scheme of ^{18}F-2-arylquinolines.

MATERIALS AND METHODS

Synthesis and Radiosynthesis of 2-Arylquinoline Derivatives

The chemical structures of 6-[(3-^{18}F-fluoro-2-hydroxy)propoxy]-2-(4-dimethylaminophenyl)quinoline (^{18}F-THK-5105), 6-[(3-^{18}F-fluoro-2-hydroxy)propoxy]-2-(4-methylaminophenyl)quinoline (^{18}F-THK-5117), 6-[(3-^{18}F-fluoro-2-hydroxy)propoxy]-2-(4-aminophenyl)quinoline (^{18}F-THK-5116), and ^{18}F-THK-523 are shown in Figure 1. ^{18}F-THK-5105, ^{18}F-THK-5116, and ^{18}F-THK-5117 were prepared from the corresponding tosylate precursors according to the scheme as indicated in the Figure 2. Details on their syntheses will be described elsewhere (S. Furumoto et al., unpublished data, 2013). Briefly, the aqueous $^{18}F^-$ contained in the K_2CO_3 solution (1.59–3.69 GBq) and Kryptofix222 (15 mg) were placed in a brown vial. Water was removed by azeotropic evaporation with acetonitrile. After being dried, the activated ^{18}F-KF/Kryptofix222 was reacted with the precursor (3 mg) in dimethylsulfoxide (0.7 mL) at 110°C for 10 min. Then, 2 M HCl was added to the solution, followed by an additional 3-min reaction for deprotection of the hydroxyl group. After neutralization with 4 M AcOK, the product was purified by semipreparative high-performance liquid chromatography (HPLC) (column: Inertsil ODS-4 [GL Sciences, Inc.]; mobile phase: 20 mM NaH_2PO_4/acetonitrile [55/45 for THK-5105 and THK-5117, 65/35 for THK-5116]; flow rate: 5.0 mL/min). The radiolabeled product was dissolved in ethanol, dimethylsulfoxide, or saline with polysobate-80 (<0.1%) for biologic evaluation.

^{18}F-THK-523 and ^{18}F-FDDNP were also prepared in a manner similar to the one described above using the corresponding tosylate precursors reported previously (*15,25,26*). ^{11}C-PiB was radiolabeled using its precursor (2-(4-aminophenyl)-6-methoxymethoxybenzothiazole) and ^{11}C-methyl triflate, as previously described (*27*).

Determination of Log P Values

Log P values were determined by the HPLC method according to the guideline of the Organisation for Economic Co-operation and Development (OECD Guideline for Testing of Chemicals: Partition Coefficient (n-octanol/water), High Performance Liquid Chromatography [HPLC] Method), with slight modification. Briefly, 12 reference compounds whose log P values ranged between 0.5 and 4.0 were analyzed by HPLC under the following conditions: HPLC, a JASCO LC-2000 Plus series (JASCO); column, Inertsil ODS-4 (4.6 × 150 mm, 5 μm; GL Sciences, Inc.); mobile phase, 20 mM NaH_2PO_4 (pH 7.4)/acetonitrile (55/45); flow rate, 1.5 mL/min; ultraviolet absorbance, 245 nm; and column temperature, 40°C. Then, a calibration curve of log (tR − t0) (tR, retention time; t0, dead time) versus log P of each reference compound was created (R^2 = 0.9469). Test compounds listed in Table 1 were also analyzed by the same HPLC method to measure log (tR − t0) values that were used for determination of log P values from the calibration curve.

In Vitro Binding Assays

Synthetic human Aβ1–42 was purchased from Peptide Institute Inc. Recombinant K18ΔK280-tau protein was obtained from Life Technologies Japan Ltd. Fibrils of

TABLE 1
Log P and Brain Uptake After Intravenous Administration of ^{18}F-Labeled Compounds in Mice

Compound	Log P	Brain uptake (%ID/g) 2 min after injection	30 min after injection	60 min after injection	Brain uptake ratio (2 min/60 min)
^{18}F-THK-523	2.40	2.72	1.47	1.46	1.86
^{18}F-THK-5105	3.03	9.20	3.61	1.00	9.20
^{18}F-THK-5116	1.57	3.36	0.75	0.57	5.89
^{18}F-THK-5117	2.32	6.06	0.59	0.26	23.1
^{18}F-FDDNP	3.71	6.23	2.02	2.14	2.91

Aβ1–42 and K18ΔK280-tau were prepared as described previously (*15*). Briefly, synthetic Aβ1–42 (200 μM) and K18Δ280K-tau (20 μM) solutions in phosphate-buffered saline (PBS) were incubated at 37° C with agitation for 3–4 d. We additionally prepared AD brain homogenates for binding assay, because the structural conformation of synthetic protein fibrils does not fully correlate with the structure of native protein deposits in the human brain. Human brain tissue was isolated from a mesial temporal frozen sample of an AD patient and homogenized in PBS. Brain tissue homogenate aliquots were taken and frozen at −80°C until used. Insoluble Aβ and tau levels were determined using a human β-amyloid enzyme-linked immunosorbent assay (ELISA) kit (Wako) and a human tau ELISA kit (Life Technologies Japan Ltd.), respectively. Next, brain homogenates and the solutions of synthetic Aβ1–42 or K18Δ280K-tau fibrils were incubated with increasing concentrations of ^{18}F-THK-5105 (0.1–250 nM). To account for nonspecific binding of ^{18}F-THK-5105, the reactions were performed in triplicate in the presence of 2 μM unlabeled THK-5105. The binding reactions were incubated for 1 h at room temperature in assay buffer (Dulbecco PBS; 0.1% bovine serum albumin). Bound radioactive compounds were separated from free radioactive compounds by filtration under reduced pressure (MultiScreen HTS Vacuum Manifold; Millipore). Filters were washed three times with assay buffer, and the radioactivity contained within the filters was counted in a γ-counter (AccuFLEX γ7000, Aloka, Tokyo, Japan). Binding data were analyzed using curve-fitting software that calculates the K_d and B_{max} (K_d is dissociation constant and B_{max} is maximum number of binding sites, respectively) using nonlinear regression (GraphPad Prism; GraphPad Software).

For inhibition studies, the assay buffer containing each compound (0.1–1,000 nM), ^{18}F-THK-5105 (1.76 nM, ~37 kBq), K18Δ280K-tau (200 nM), and 0.1% bovine serum albumin was incubated at room temperature for 1 h. Nonspecific binding was determined in the presence of 10 μM THK-5105. The mixture was filtered through Multiscreen HTS 96-well filtration plates, followed by washing three times with PBS (0.1% bovine serum albumin), and the filters containing bound ^{18}F ligand were counted in a γ-counter. The percentage of bound radioligand at each concentration was measured in triplicate and then plotted against the inhibitor concentration. Half-maximal inhibitory concentration values were determined from the displacement curves using the GraphPad Prism software. Inhibition constant (K_i) values were calculated from the half-maximal inhibitory concentration values using the Cheng–Prusoff equation (*28*).

TABLE 2
K_d and B_{max} Values of ^{18}F-THK-5105 for Synthetic Tau and $Aβ_{1–42}$ Fibrils

Protein	K_{d1}	B_{max1}	K_{d2}	B_{max2}
Tau	1.45	6.89	7.40	20.05
$Aβ_{1–42}$	35.9	61.6		

K_d are in nM and Bmax are in pmol ^{18}F-THK-5105/nmol fibrils.

Tissue Staining

Experiments were performed under the regulations of the ethics committee of Tohoku University School of Medicine. Paraffin-embedded hippocampal brain sections from an autopsy-confirmed AD case (78-y-old woman) were used for tissue staining with THK-5105. Brain sections were obtained from Fukushimura Hospital. After deparaffinization, autofluorescence quenching was performed as previously described (*29*). Quenched tissue sections were immersed for 10 min in a 100-μM THK-5105 solution containing 50% ethanol. Sections were then dipped briefly into water, rinsed in PBS, coverslipped with FluorSave Reagent (Calbiochem), and examined using an Eclipse microscope (Nikon) equipped with a blue-violet filter (excitation, 400–440 nm; dichroic mirror, 455 nm; barrier filter, 470 nm). Sections stained with THK-5105 were subsequently immunostained with the AT8 anti-tau antibody (diluted 1:20; Innogenetics). After incubation at 4°C in the primary antibody for 16 h, sections were processed by the avidin-biotin method using a Pathostain ABC-POD(M) Kit (Wako) and diaminobenzidine as a chromogen. Sections were additionally stained using a modified Gallyas–Braak method (pretreatment with 0.3% potassium permanganate for 10 min, followed by 0.1% oxalic acid for 3 min) (*30*).

Autoradiography of Human Brain Sections

For the autoradiographic study, 8-μm-thick paraffin-embedded brain sections from a healthy control (62-y-old man) and 2 AD patients (69-y-old man and 92-y-old woman) were used. After deparaffinization, sections were incubated for 10 min at room temperature with radiolabeled compounds (0.5 MBq/mL) and washed briefly with water and 50% ethanol. After being dried, the labeled sections were exposed overnight to a BAS-III imaging plate (Fuji Film). The autoradiographic images were obtained using a BAS-5000 phosphoimaging instrument (Fuji Film). The neighboring sections were stained

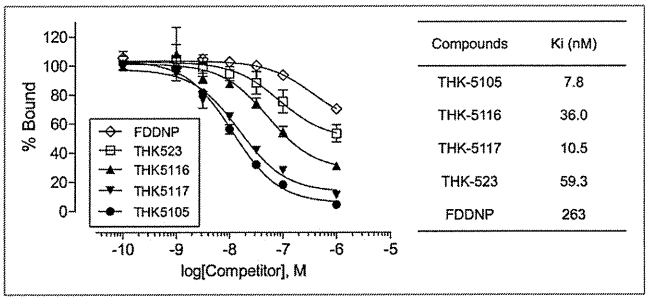

FIGURE 3. Competitive inhibition of ^{18}F-THK-5105 binding by 2-arylquinolines and FDDNP to tau protein fibrils. K_i values for inhibition of ^{18}F-THK-5105 binding to tau are shown.

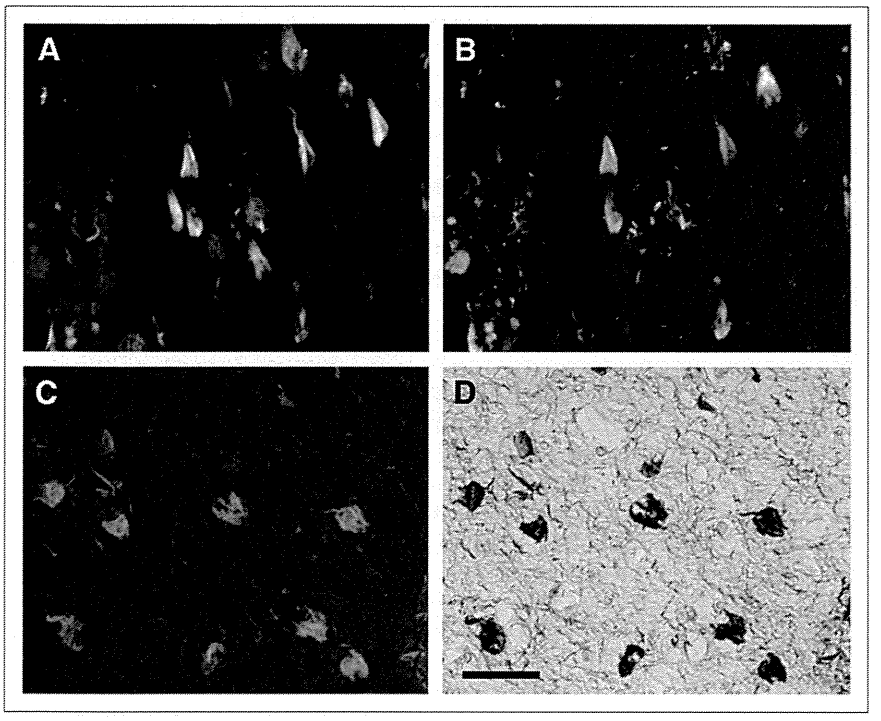

FIGURE 4. Neuropathologic staining of brain sections from AD patients. Neurofibrillary tangles and neuropil threads were clearly stained with THK-5105 (A and C). These stainings were consistent with tau immunostaining (B) and Gallyas–Braak staining (D) in same sections. Bar = 50 μm.

using a modified Gallyas–Braak method or immunostained using the AT8 anti-tau monoclonal antibody (diluted 1:20; Innogenetics), the 4G8 Aβ antibody (diluted 1:100; Signet), or the 6F/3D Aβ antibody (diluted 1:50; Dako). For correlational analysis of the autoradiographic and immunohistochemical images, 36 circular regions of interest (the area of each region of interest was ~7 mm^2) were placed on the gray matter of the hippocampus, parahippocampal gyrus, fusiform gyrus, temporal gyri (superior, middle, and inferior), insula, pre- and postcentral gyri, superior frontal gyrus, paracentral lobule, and cingulate gyrus. The percentage area of positive signals in each region of interest was calculated using ImageJ software (National Institutes of Health). A correlational analysis between percentage areas of tracer binding and positive immunostaining was performed using Pearson simple correlation.

Biodistribution in Mice

The experimental protocol of animal study was approved by the Ethics Committee of Tohoku University School of Medicine. ^{18}F-labeled tracers (1.1–6.3 MBq) were injected into the tail vein of male ICR mice (n = 20; mean weight, 28–32 g). Mice were then sacrificed by decapitation at 2, 10, 30, 60, and 120 min after injection. The brain, blood, liver, kidney, and femur were removed and weighed, and radioactivity was counted with an automatic γ-counter. The percentage injected dose per gram of tissue (%ID/g) was calculated by comparing tissue counts to tissue weight. Each %ID/g value is expressed as a mean ± SD of 4 separate experiments.

Animal Toxicity Studies

A 14-d toxicity study with intravenous administration of a single dose of THK-5105 and THK-5117 was performed using Sprague–Dawley rats and ICR mice. Briefly, the study included 3 groups of male and female rats and mice that were administered 0 (group 1), 0.1 (group 2), and 1 (group 3) mg/kg of test article (10% dimethylsulfoxide/90% distilled water) per rat or mouse by intravenous injection on study day 1. The study included clinical observations plus body weight measurements for a 14-d observation period. Hematology and pathologic examinations were conducted on study days 2 and 15. Detailed necropsies with external examinations were also performed.

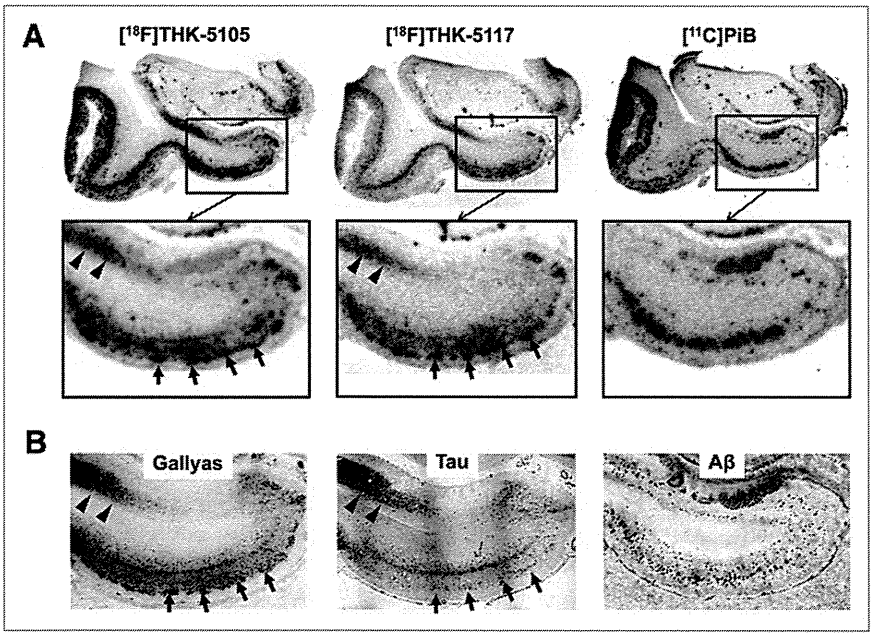

FIGURE 5. (A) Autoradiographic images of ^{18}F-THK-5105, ^{18}F-THK-5117, and ^{11}C-PiB binding in mesial temporal section from AD patient. (B) Gallyas–Braak silver staining (left) and immunostaining with anti-tau (center) and anti-Aβ (right) antibodies in adjacent brain sections. Arrowheads = CA1 area of hippocampus; longer arrows = entorhinal cortex.

Receptor Binding Assays

Receptor binding screens were conducted by Sekisui Medical Inc. Binding inhibition effects of 1 μM THK-5105 and THK-5117 were evaluated in competitive radioligand assays against 60 common neurotransmitter receptors, ion channels, and transporters. Percentage inhibition ratios were calculated by the following equation: inhibition ratio (%) = $[1 - (B - N)/(B_0 - N)] \times 100$, where N is the nonspecific bound radioactivity, and B and B_0 are the bound radioactivity in the presence and absence of tested compounds, respectively. Data are expressed as the mean values of duplicate samples.

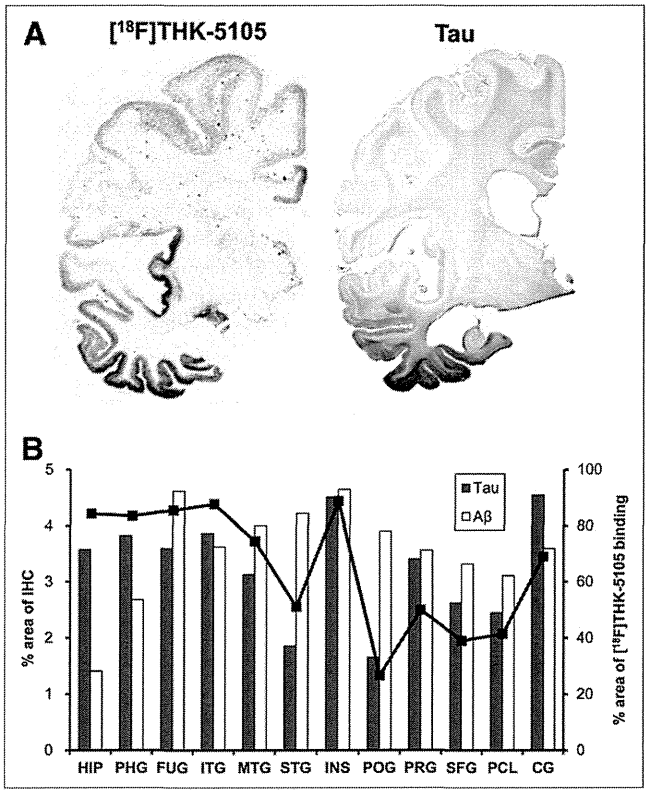

FIGURE 6. (A) Autoradiography of hemibrain sections from AD patient with ^{18}F-THK-5105 and tau immunostaining in neighboring section. (B) Region-of-interest analysis indicated that percentage areas of ^{18}F-THK-5105 binding (line plots) were significantly correlated with percentage areas of tau immunostaining (gray bars) but not with that of Aβ immunostaining (white bars). CG = cingulate gyrus; HIP = hippocampus; FUG = fusiform gyrus; IHC = immunohistochemistry; INS = insula; ITG = inferior temporal gyrus; MTG = middle temporal gyrus; PCL = paracentral lobule; PHG = parahippocampal gyrus; POG = postcentral gyrus; PRG = precentral gyrus; SFG = superior frontal gyrus; STG = superior temporal gyrus.

RESULTS

Radiosynthesis

All radiolabeled compounds were obtained in greater than 97% radiochemical purities after HPLC purification. The decay-corrected average radiochemical yields of ^{18}F-THK-523, ^{18}F-THK-5105, ^{18}F-THK-5116, ^{18}F-THK-5117, and ^{18}F-FDDNP were 58%, 48%, 41%, 48%, and 22%, respectively. The specific activities of ^{18}F-labeded compounds ranged from 37 to 110 GBq/μmol, corrected at the end of synthesis. The mean specific activity of ^{11}C-PiB was 35 GBq/μmol.

In Vitro Binding Assays

The binding properties of phenylquinoline derivatives to tau fibrils was investigated and compared with Aβ1–42 fibrils. Although only a single class of ^{18}F-THK-5105 binding sites was identified on Aβ1–42 fibrils, 2 classes of ^{18}F-THK-5105 binding sites were identified on K18Δ280-tau fibrils. As shown in Table 2, the K_d for the first class of K18Δ280-tau binding sites was 1.45 nM, indicating higher binding affinity to tau fibrils than to Aβ1–42 fibrils (K_d = 35.9 nM). Further, competitive binding assays with ^{18}F-THK-5105 displayed high binding affinity of phenylquinoline derivatives to tau fibrils (Fig. 3). The K_i for THK-5117 was 10.5 nM, indicating that THK-5117 has higher binding affinity for tau fibrils than THK-523 (K_i = 59.3 nM). In contrast, the K_i for FDDNP was 263 nM. In binding assays using mesial temporal brain homogenates containing a high density of tau (1,075 pmol/g) and moderate density of Aβ (434 pmol/g), both ^{18}F-THK-5105 (K_d = 2.63 nM; B_{max} = 358 pmol/g of tissue) and ^{18}F-THK-5117 (K_d = 5.19 nM; B_{max} = 338 pmol/g of tissue) showed higher affinity for mesial temporal brain homogenates than ^{18}F-THK-523 (K_d = 86.5 nM; B_{max} = 647.1 pmol/g of tissue) (Supplemental Fig. 1; supplemental materials are available online only at http://jnm.snmjournals.org).

Tissue Staining and Autoradiography

The selective binding ability of the compounds was further examined using AD brain sections. The fluorescent compound THK-5105 clearly stained NFTs and neuropil threads in the hippocampal section of an AD patient (Fig. 4A). Selective binding of this compound with tau pathology was confirmed by comparing with the results of tau immunohistochemistry for the same sections (Fig. 4B). In contrast, SPs were faintly stained with THK-5105. Further, we compared findings of THK-5105 staining with those of Gallyas–Braak silver staining, a conventional technique used to visualize tau pathology in the AD brain (Figs. 4C and 4D), and the binding of THK-5105 to NFTs and neuropil threads was confirmed. The images of staining with THK-5116 and THK-5117 were similar to those with THK-5105 (data not shown).

To investigate the binding ability of ^{18}F-THK-5105 and ^{18}F-THK-5117 to NFTs at tracer doses, in vitro autoradiography was performed in postmortem AD brain sections, and the findings were compared with Gallyas–Braak staining and immunohistochemistry. In the mesial temporal sections, laminar distributions of ^{18}F-THK-5105 and ^{18}F-THK-5117 were observed in the deep layer of gray matter (Fig. 5A). A high density of tracer accumulation was observed in the CA1 area of the hippocampus, which is reported as the most frequent site for NFTs in AD (*31*). These tracer distributions coincided with Gallyas–Braak staining and tau immunostaining (Fig. 5B) but not with the distribution of ^{11}C-PiB (Fig. 5A) and Aβ immunostaining (Fig. 5B). In contrast, no significant accumulation of ^{18}F-THK-5105 and ^{18}F-THK-5117 was observed in the hippocampus of the healthy control subject (Supplemental Fig. 2). ^{18}F-THK-5116 failed to give a specific signal in the AD brain sections (data not shown).

To further assess the regional differences of tracer binding in the AD brain, ^{18}F-THK-5105 autoradiography was conducted using AD hemibrain sections and compared with the Aβ PET tracer ^{11}C-PiB (*32*). ^{18}F-THK-5105 densely accumulated in the gray matter of the hippocampus, parahippocampal gyrus, fusiform gyrus, inferior and middle temporal gyri, insula, and cingulate gyrus (Fig. 6A), regions known for the abundance of tau pathology in AD (*33*). In contrast, tracer binding in the parietal areas was modest. The pattern of tracer distribution correlated with the known distribution of tau pathology (Fig. 6A) but not with the known distribution of Aβ or the binding of ^{11}C-PiB (data not shown). In addition, quantitative analyses of these images demonstrated a significant correlation of ^{18}F-THK-5105 binding with tau immunostained areas but not with the areas of Aβ immunostaining (Fig. 6B; Supplemental Fig. 3). In contrast, ^{11}C-PiB bindings showed a good correlation with Aβ deposition but not with tau deposition (Supplemental Fig. 3).

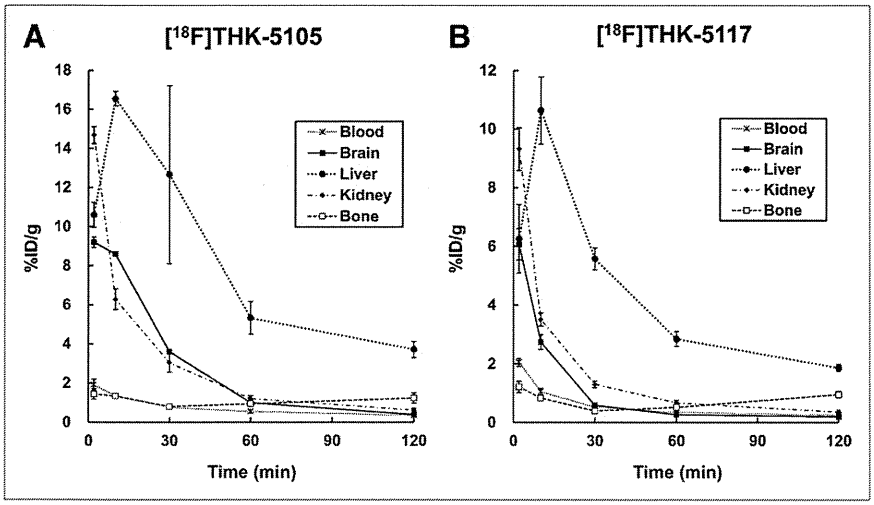

FIGURE 7. Time–activity curves after intravenous administration of ^{18}F-THK-5105 (A) and ^{18}F-THK-5117 (B) in mice.

Pharmacokinetics in Mice

All tested compounds exhibited sufficient amounts of tracer uptake in the mouse brain immediately after intravenous administration. Compared with ^{18}F-THK-523, new compounds showed significantly higher brain uptake at 2 min after injection (Table 1). ^{18}F-THK-5105 showed the highest brain uptake. In addition, clearance of these derivatives from normal brain tissue was faster than that of ^{18}F-THK-523 and ^{18}F-FDDNP (Table 1). The brain uptake ratio at 2 versus 60 min was highest for ^{18}F-THK-5117, followed by ^{18}F-THK-5105, ^{18}F-THK-5116, ^{18}F-FDDNP, and ^{18}F-THK-523. After injection of ^{18}F-THK-5105 and ^{18}F-THK-5117, the regional tracer uptake in the liver was highest at 10 min after injection, and the tracer was then slowly washed out from the body (Fig. 7). Compared with ^{18}F-THK-5105, ^{18}F-THK-5117 tended to have faster clearance from the brain, blood, liver, and kidney. No remarkable accumulation of ^{18}F-THK-5105 and ^{18}F-THK-5117 was observed in the bone.

Animal Toxicity Studies

A single intravenous administration of THK-5105 and THK-5117 at 1 mg/kg, equivalent to 100,000-fold the intended clinical dose for humans, caused no systemic toxicity in rats or mice. There were no unscheduled deaths or morbidity detected in this study. During the experimental period, the body weight of all animals increased normally, and no treatment-related changes were noted in any animals. There were no major clinical, biochemical, or histopathologic findings associated with the administration of THK-5105 and THK-5117.

Receptor Binding Assays

Binding inhibition of THK-5105 and THK-5117 was assessed in competitive radioligand binding assays against 60 common neurotransmitter receptors, ion channels, and transporters. As a result, no remarkable inhibition (<50%) was observed for various receptors, ion channels, and transporters at 1-μM concentrations of THK-5105 and THK-5117.

DISCUSSION

These findings suggest that ^{18}F-THK-5105 and ^{18}F-THK-5117 are promising candidates as tau imaging PET probes. Although previous saturation analysis showed the high binding affinity of ^{18}F-THK-523 for tau fibrils (K_d = 1.67 nM), the current competition assay demonstrated relatively lower binding affinity of THK-523 for tau fibrils (K_i = 59.3 nM) than THK-5105 (K_i = 7.8 nM) and THK-5117 (K_i = 10.5 nM). ^{18}F-THK-5105 showed higher affinity for tau pathology than for Aβ pathology in AD brain sections. Most amyloid imaging agents potentially bind to both tau and Aβ fibrils, because both protein fibrils share a common β-sheet secondary structure. To ensure the binding specificity of these compounds as tau-selective PET probes, the binding affinity to Aβ fibrils should be below the in vivo detection threshold. In vitro binding assays indicated that the binding affinity of ^{18}F-THK-5105 for Aβ fibrils (K_d = 35.9 nM) was 25 times lower than for tau fibrils (K_d = 1.45 nM). This K_d would allow selective detection of tau pathology, because the usual required K_d values for imaging Aβ are below 20 nM (*34*). However, the required K_d value for imaging tau deposits is still unknown. Considering that the concentrations of tau are about an order of magnitude lower than those of Aβ, the K_d value for tau should be well below 20 nM, in the low nanomolar range, to allow sensitive detection of tau pathology. In that respect, the binding affinities of both ^{18}F-THK-5105 and ^{18}F-THK-5117 to tau fibrils may be sufficient for in vivo detection of tau pathology in the brain. However, in vitro binding assay data should be carefully interpreted, because the structural conformation of synthetic tau fibrils does not fully correlate with the structure of NFTs and neuropil threads in the human brain. Actually, ^{18}F-THK-523 showed substantially lower affinity for AD brain homogenates (Kd = 86.5 nM) than for synthetic tau protein fibrils (Kd = 1.67 nM) (*15*). In the future, in vitro binding data should be compared with in vivo PET data to determine the required K_d value for in vivo tau detection.

In vitro assays using human brain samples are considered more reliable for evaluating the binding selectivity of radiotracers to tau and Aβ pathology at tracer doses. Autoradiography studies using human brain sections demonstrated the preferential binding of ^{18}F-THK-5105 and ^{18}F-THK-5117 to tau protein deposits in the AD brain. We observed a high density of ^{18}F-THK-5105 and ^{18}F-THK-5117 binding in the CA1 region of AD hippocampus, which contained substantial amounts of NFTs and neuropil threads. In addition, these tracers clearly visualized the laminar distribution of tau in the pri-α layer of the transentorhinal and temporal cortices, which is typically observed in the AD brain (*5*). The distribution pattern of THK tracer binding in AD brains was different from that of the Aβ imaging probe PiB and BF-227, which showed diffuse punctate distribution in broad neocortical gray matter and less tracer distribution in the mesial temporal region. These findings strongly suggest that binding properties of ^{18}F-THK-5105 and ^{18}F-THK-5117 are different from those of currently available Aβ PET probes. Compared with ^{18}F-THK-523 (*17*), both ^{18}F-THK-5105 and ^{18}F-THK-5117 showed higher contrast of tau pathology in autoradiographic images. These findings most likely reflect the increased binding affinity to tau by methylation of the amino group, as indicated by in vitro binding assays.

Similar findings were previously reported in an arylbenzothiazole derivative (*35*). Compared with ^{18}F-THK-5105, ^{18}F-THK-5117 showed lesser tracer binding in the gray matter containing high density of Aβ plaques, suggesting low binding affinity to Aβ and high selectivity to tau. ^{18}F-THK-5105 tends to show higher signals in the gray matter, and some of the images of ^{18}F-THK-5105 binding showed the patchy pattern as observed for ^{11}C-PiB binding. One possible reason for this is the binding of ^{18}F-THK-5105 to tau protein in dystrophic neurites. Another possible reason is binding of ^{18}F-THK-5105 to Aβ fibrils. However, the latter explanation seems unlikely given that ^{18}F-THK-5105 binding, as clearly shown in Figure 6, was correlated with tau, and not Aβ, deposits.

In vitro binding assays using AD brain homogenates are generally used to measure the binding affinity of Aβ imaging radiotracers to SPs or NFTs and the number of binding sites in real AD pathology (*36*). For most of the useful Aβ imaging radiotracers, the reported K_d or K_i values for neocortical brain samples are below 10 nM (*36,37*). In this study, the K_d values for high-affinity sites of AD mesial temporal homogenates were 2.63 nM for ^{18}F-THK-5105 and 5.19 nM for ^{18}F-THK-5117. These binding affinities were higher than that for ^{18}F-THK-523 and appear to be sufficient for the in vivo detection of AD pathology in the mesial temporal region at tracer doses. Furthermore, the B_{max}/K_d ratios of ^{18}F-THK-5105 and ^{18}F-THK-5117 for AD brain homogenates were 136.1 and 65.1, respectively, which fulfills the criteria (B_{max}/K_d ratio > 10) for a good neuroimaging agent (*35*).

The optimization of pharmacokinetics is an important aspect in the development of a PET tracer (*38*). ^{18}F-THK-5105, ^{18}F-THK-5116, and ^{18}F-THK-5117 fulfilled the criteria of appropriate log P value (log P = 1–3) for brain entry (*39*). In mice, these tracers showed sufficient brain uptake and rapid washout from normal brain tissue. ^{18}F-THK-5105 and ^{18}F-THK-5117 exhibited high initial brain uptake in normal mice (>6 %ID/g at 2 min). These values, which are equivalent to over 100% injected dose index in a 25-g mouse, meet the prerequisites for useful PET imaging agents (*34*). The 2- to 60-min ratio of radioactivity concentrations for ^{18}F-THK-5117 was 23.1, indicating faster washout from normal brain for these compounds than for other currently available ^{18}F-labeled tracers such as ^{18}F-FDDNP (2.91), ^{18}F-florbetaben (4.83) (*40*), and ^{18}F-florbetapir (3.90) (*37*). Compared with ^{18}F-THK-523, ^{18}F-THK-5116 washed out faster from normal brain tissue of mice, indicating that the hydroxylation of the fluoroalkoxy group improves pharmacokinetics in mice. However ^{18}F-THK-5116 is not a suitable compound for clinical application, because of its lower initial brain uptake and binding affinity than the other 2 compounds.

CONCLUSION

^{18}F-THK-5105 and ^{18}F-THK-5117 should be considered as promising candidates for PET tau imaging radiotracers. Future clinical studies will clarify the usefulness of these radiotracers for the early detection of AD tau pathology.

DISCLOSURE

The costs of publication of this article were defrayed in part by the payment of page charges. Therefore, and solely to indicate this fact, this article is hereby marked "advertisement" in accordance with 18 USC section 1734. This study was supported by the research fund from GE Healthcare; the Industrial Technology Research Grant Program of the NEDO in Japan (09E51025a); Health and Labor Sciences Research grants from the Ministry of Health, Labor, and Welfare of Japan; and a Grant-in-Aid for Scientific Research (B) (23390297) and "Japan Advanced Molecular Imaging Program (J-AMP)" of the Ministry of Education, Culture, Sports, Science and Technology (MEXT), Japan. No other potential conflict of interest relevant to this article was reported.

REFERENCES

1. Organisation for Economic Co-operation and Development (OECD). *Understanding the Brain: The Birth of a Learning Science*. Paris, France: OECD Publishing, 2007.
2. Hardy J, Selkoe DJ. The amyloid hypothesis of Alzheimer's disease: progress and problems on the road to therapeutics. *Science*. 2002;297:353–356.
3. Lichtenberg B, Mandelkow EM, Hagestedt T, Mandelkow E. Structure and elasticity of microtubule-associated protein tau. *Nature*. 1988:334:359–362.
4. Holzer M, Holzapfel HP, Zedlick D, Bruckner MK, Arendt T. Abnormally phosphorylated tau protein in Alzheimer's disease: heterogeneity of individual regional distribution and relationship to clinical severity. *Neuroscience*. 1994;63: 499–516.
5. Braak H, Braak E. Neuropathological stageing of Alzheimer-related changes. *Acta Neuropathol*. 1991;82:239–259.
6. Bondareff W, Mountjoy CQ, Roth M, Hauser DL. Neurofibrillary degeneration and neuronal loss in Alzheimer's disease. *Neurobiol Aging*. 1989;10:709–715.
7. Bobinski M, Wegiel J, Wisniewski HM, et al. Neurofibrillary pathology: correlation with hippocampal formation atrophy in Alzheimer disease. *Neurobiol Aging*. 1996;17:909–919.
8. Guillozet AL, Weintraub S, Mash DC, Mesulam MM. Neurofibrillary tangles, amyloid, and memory in aging and mild cognitive impairment. *Arch Neurol*. 2003;60:729–736.
9. Gómez-Isla T, Price JL, McKeel DW Jr., Morris JC, Growdon JH, Hyman BT. Profound loss of layer II entorhinal cortex neurons occurs in very mild Alzheimer's disease. *J Neurosci*. 1996;16:4491–4500.
10. Okamura N, Suemoto T, Furumoto S, et al. Quinoline and benzimidazole derivatives: candidate probes for in vivo imaging of tau pathology in Alzheimer's disease. *J Neurosci*. 2005;25:10857–10862.
11. Rojo LE, Alzate-Morales J, Saavedra IN, Davies P, Maccioni RB. Selective interaction of lansoprazole and astemizole with tau polymers: potential new clinical use in diagnosis of Alzheimer's disease. *J Alzheimers Dis*. 2010;19:573–589.
12. Ono M, Hayashi S, Matsumura K, et al. Rhodanine and thiohydantoin derivatives for detecting tau pathology in Alzheimer's brains. *ACS Chem Neurosci*. 2011;2:269–275.
13. Jensen JR, Cisek K, Funk KE, Naphade S, Schafer KN, Kuret J. Research towards tau imaging. *J Alzheimers Dis*. 2011;26(suppl 3):147–157.
14. Zhang W, Arteaga J, Cashion DK, et al. A highly selective and specific PET tracer for imaging of tau pathologies. *J Alzheimers Dis*. 2012;31:601–612.
15. Fodero-Tavoletti MT, Okamura N, Furumoto S, et al. ^{18}F-THK523: a novel in vivo tau imaging ligand for Alzheimer's disease. *Brain*. 2011:134:1089–1100.
16. Villemagne VL, Furumoto S, Fodero-Tavoletti MT, et al. The challenges of tau imaging. *Future Neurol*. 2012;7:409–421.
17. Harada R, Okamura N, Furumoto S, et al. Comparison of the binding characteristics of [^{18}F]THK-523 and other amyloid imaging tracers to Alzheimer's disease pathology. *Eur J Nucl Med Mol Imaging*. 2013;40:125–132.
18. Small GW, Agdeppa ED, Kepe V, Satyamurthy N, Huang SC, Barrio JR. In vivo brain imaging of tangle burden in humans. *J Mol Neurosci*. 2002;19:323–327.
19. Agdeppa ED, Kepe V, Liu J, et al. Binding characteristics of radiofluorinated 6-dialkylamino-2-naphthylethylidene derivatives as positron emission tomography imaging probes for beta-amyloid plaques in Alzheimer's disease. *J Neurosci*. 2001;21:RC189.
20. Thompson PW, Ye L, Morgenstern JL, et al. Interaction of the amyloid imaging tracer FDDNP with hallmark Alzheimer's disease pathologies. *J Neurochem*. 2009;109:623–630.
21. Tolboom N, Yaqub M, van der Flier WM, et al. Detection of Alzheimer pathology in vivo using both ^{11}C-PIB and ^{18}F-FDDNP PET. *J Nucl Med*. 2009;50: 191–197.
22. Shoghi-Jadid K, Small GW, Agdeppa ED, et al. Localization of neurofibrillary tangles and beta-amyloid plaques in the brains of living patients with Alzheimer disease. *Am J Geriatr Psychiatry*. 2002;10:24–35.

23. Näslund J, Haroutunian V, Mohs R, et al. Correlation between elevated levels of amyloid beta-peptide in the brain and cognitive decline. *JAMA.* 2000;283: 1571–1577.
24. Mukaetova-Ladinska EB, Harrington CR, Roth M, Wischik CM. Biochemical and anatomical redistribution of tau protein in Alzheimer's disease. *Am J Pathol.* 1993;143:565–578.
25. Liu J, Kepe V, Zabjek A, et al. High-yield, automated radiosynthesis of 2-(1-{6-[(2-[^{18}F]fluoroethyl)(methyl)amino]-2-naphthyl}ethylidene)malononitrile ([^{18}F] FDDNP) ready for animal or human administration. *Mol Imaging Biol.* 2007;9:6–16.
26. Fodero-Tavoletti MT, Mulligan RS, Okamura N, et al. In vitro characterisation of BF227 binding to alpha-synuclein/Lewy bodies. *Eur J Pharmacol.* 2009;617:54–58.
27. Wilson AA, Garcia A, Chestakova A, Kung H, Houle S. A rapid one-step radiosynthesis of the beta-amyloid imaging radiotracer N-methyl-[C-11]2-(4′-methylaminophenyl)-6-hydroxybenzothiazole ([C-11]-6-OH-BTA-1). *J Labelled Comp Radiopharm.* 2004;47:679–682.
28. Cheng Y, Prusoff WH. Relationship between the inhibition constant (Ki) and the concentration of inhibitor which causes 50 per cent inhibition (IC50) of an enzymatic reaction. *Biochem Pharmacol.* 1973;22:3099–3108.
29. Okamura N, Suemoto T, Shimadzu H, et al. Styrylbenzoxazole derivatives for in vivo imaging of amyloid plaques in the brain. *J Neurosci.* 2004;24: 2535–2541.
30. Ikeda K, Akiyama H, Kondo H, Haga C. A study of dementia with argyrophilic grains. Possible cytoskeletal abnormality in dendrospinal portion of neurons and oligodendroglia. *Acta Neuropathol.* 1995;89:409–414.
31. Bouras C, Hof PR, Giannakopoulos P, Michel JP, Morrison JH. Regional distribution of neurofibrillary tangles and senile plaques in the cerebral cortex of elderly patients: a quantitative evaluation of a one-year autopsy population from a geriatric hospital. *Cereb Cortex.* 1994;4:138–150.
32. Kudo Y, Okamura N, Furumoto S, et al. 2-(2-[2-Dimethylaminothiazol-5-yl] ethenyl)-6- (2-[fluoro]ethoxy)benzoxazole: a novel PET agent for in vivo detection of dense amyloid plaques in Alzheimer's disease patients. *J Nucl Med.* 2007;48:553–561.
33. Braak H, Alafuzoff I, Arzberger T, Kretzschmar H, Del Tredici K. Staging of Alzheimer disease-associated neurofibrillary pathology using paraffin sections and immunocytochemistry. *Acta Neuropathol.* 2006;112:389–404.
34. Mathis CA, Wang Y, Klunk WE. Imaging beta-amyloid plaques and neurofibrillary tangles in the aging human brain. *Curr Pharm Des.* 2004;10:1469–1492.
35. Mathis CA, Wang Y, Holt DP, Huang GF, Debnath ML, Klunk WE. Synthesis and evaluation of ^{11}C-labeled 6-substituted 2-arylbenzothiazoles as amyloid imaging agents. *J Med Chem.* 2003;46:2740–2754.
36. Klunk WE, Wang Y, Huang GF, et al. The binding of 2-(4′-methylaminophenyl) benzothiazole to postmortem brain homogenates is dominated by the amyloid component. *J Neurosci.* 2003;23:2086–2092.
37. Choi SR, Golding G, Zhuang Z, et al. Preclinical properties of ^{18}F-AV-45: a PET agent for Abeta plaques in the brain. *J Nucl Med.* 2009;50:1887–1894.
38. Furumoto S, Okamura N, Iwata R, Yanai K, Arai H, Kudo Y. Recent advances in the development of amyloid imaging agents. *Curr Top Med Chem.* 2007;7:1773–1789.
39. Waterhouse RN. Determination of lipophilicity and its use as a predictor of blood-brain barrier penetration of molecular imaging agents. *Mol Imaging Biol.* 2003;5:376–389.
40. Zhang W, Oya S, Kung MP, Hou C, Maier DL, Kung HF. F-18 Polyethyleneglycol stilbenes as PET imaging agents targeting Abeta aggregates in the brain. *Nucl Med Biol.* 2005;32:799–809.

J Gastroenterol (2014) 49:231–238
DOI 10.1007/s00535-013-0797-y

The Japanese Society of Gastroenterology

ORIGINAL ARTICLE—ALIMENTARY TRACT

Long-term incidence and characteristics of intestinal failure in Crohn's disease: a multicenter study

Kazuhiro Watanabe · Iwao Sasaki · Kouhei Fukushima · Kitaro Futami · Hiroki Ikeuchi · Akira Sugita · Riichiro Nezu · Tsunekazu Mizushima · Shingo Kameoka · Masato Kusunoki · Kazuhiko Yoshioka · Yuji Funayama · Toshiaki Watanabe · Hisao Fujii · Mamoru Watanabe

Received: 28 December 2012 / Accepted: 14 March 2013 / Published online: 7 April 2013

Abstract
Background The aim of this study was to clarify the risk and characteristics of intestinal failure (IF) in patients with Crohn's disease (CD).
Methods The present study was a retrospective study in 12 hospitals. CD patients who underwent initial surgery at any of the 12 hospitals between 1970 and 2009 were collected ($n = 1{,}703$). Those who developed IF were reviewed ($n = 68$), and the cumulative risk of IF was analyzed by the Kaplan–Meier method. In addition, IF patients who underwent initial surgery at other hospitals and were then treated at any of the 12 hospitals were also reviewed ($n = 33$). Thus, a total of 101 IF patients were collected, and the cumulative risk of IF-related death was analyzed.
Results The cumulative risk of IF after the initial surgery was 0.8 % (5 years), 3.6 % (10 years), 6.1 % (15 years), and 8.5 % (20 years). In CD patients with IF, mean age at initial surgery, IF occurrence, and present age at the time of the study were 28.2, 38.2, and 46.1 years, respectively. The mean number of surgeries per patient was 3.3. The mean length of the remnant small bowel was 163 cm. Twelve IF patients (12 %) had died and the cumulative risk of IF-related death by the time from the occurrence of IF was 1.1 % (3 years), 3.7 % (5 years), 6.5 % (7 years), and 8.9 % (10 years).

The present study was performed as a project study under the Surgical Research Group, the Research Committee of Inflammatory Bowel Disease, Ministry of Health, Labour and Welfare of Japan.

A portion of the data from the present study was presented as a symposium session at the 112th Annual Congress of Japan Surgical Society, April 12–14, 2012, Makuhari, Japan.

K. Watanabe (✉) · I. Sasaki · K. Fukushima
Department of Surgery, Tohoku University Hospital, 1-1 Seiryo-machi, Aoba-ku, Sendai, Miyagi, Japan
e-mail: k-wata@surg1.med.tohoku.ac.jp

K. Fukushima
Laboratory of GI Tract Reconstruction, Tohoku University Graduate School of Biomedical Engineering, Sendai, Japan

K. Fukushima
Department of Molecular and Surgical Pathophysiology, Tohoku University Graduate School of Medicine, Sendai, Japan

K. Futami
Department of Surgery, Fukuoka University Chikushi Hospital, Fukuoka, Japan

H. Ikeuchi
Inflammatory Bowel Disease Center, Hyogo College of Medicine, Nishinomiya, Japan

A. Sugita
Department of Surgery, Yokohama Municipal Citizen's Hospital, Yokohama, Japan

R. Nezu
Department of Surgery, Osaka Rosai Hospital, Sakai, Japan

T. Mizushima
Department of Gastroenterological Surgery, Osaka University Hospital, Suita, Japan

S. Kameoka
Department of Surgery II, Tokyo Women's Medical University, Tokyo, Japan

M. Kusunoki
Department of Gastrointestinal and Pediatric Surgery, Mie University Hospital, Tsu, Japan

Conclusion The occurrence of IF and IF-related death in CD patients is not rare over the long term. There is a pressing need to develop strategies for the prevention and management of IF.

Keywords Crohn's disease · Intestinal failure · Short bowel syndrome · Home parenteral nutrition · Surgery

Introduction

Crohn's disease (CD) is a chronic inflammatory gastrointestinal disorder with a high recurrence rate. It is estimated that up to 80 % of patients with CD will require at least one intestinal surgery during their course [1–4]. The rates of recurrence requiring re-operation from the first surgery are reported to range from 16 to 36 % at 5 years and from 28 to 55 % at 10 years [3–6]. Although medical and surgical management aims to prevent recurrence and minimize the extent of resection [7], CD patients often require multiple surgeries, which increases the risk for intestinal failure (IF).

The term IF was originally defined by Fleming and Remington as a reduction in functioning gut mass below the minimum necessary for adequate digestion and absorption of nutrients [8]. Initially, this definition was often used to describe patients who require home parenteral nutrition (HPN) to survive, without taking into account the patients who simply require fluid [9]. Recently, the definition has been broadened, and an international consensus group proposed that IF be characterized by the inability to maintain protein-energy, fluid, electrolyte, or micronutrient balance, which results from obstruction, dysmotility, surgical resection, congenital defect, or disease-associated loss of absorption [10].

K. Yoshioka
Department of Surgery, Kansai Medical University Kouri Hospital, Osaka, Japan

Y. Funayama
Department of Colorectal Surgery, Tohoku Rosai Hospital, Sendai, Japan

T. Watanabe
Department of Surgical Oncology, The University of Tokyo, Tokyo, Japan

H. Fujii
Department of Endoscopy, Nara Medical University Hospital, Kashihara, Japan

M. Watanabe
Department of Gastroenterology, Tokyo Medical and Dental University, Tokyo, Japan

Among patients with CD who receive long-term treatment, IF is one of the most serious complications. However, there have been few reports concerning the occurrence rate and characteristics of IF in CD patients. The aim of the present study was to clarify the risk and characteristics of IF in CD patients after intestinal surgery.

Methods

Participating hospitals

This retrospective study was performed at the following 12 Japanese hospitals, which were participants in the study group of inflammatory bowel disease, sponsored by the Japanese Ministry of Health, Labour and Welfare: Tohoku University Hospital, Fukuoka University Chikushi Hospital, Hyogo Medical University Hospital, Yokohama Municipal Citizen's Hospital, Osaka Rosai Hospital, Osaka University Hospital, Tokyo Women's Medical University Hospital, Mie University Hospital, Kansai Medical University Hirakata Hospital, Tohoku Rosai Hospital, Teikyo University Hospital, and Nara Medical University Hospital.

Definition of IF

The definition of IF in the present study was based on the proposed definition by the international consensus group [10]. CD patients who required intravenous infusion therapy at least twice per week for a period of more than 1 year because of inability to maintain protein-energy, fluid, electrolyte, or micronutrient balance, which resulted from surgical resection, were defined as having IF in the present study. Patients who received intravenous infusion therapy for bowel inflammation, bowel stenosis, fistula, abscess, and/or anal disease were excluded. In terms of the type of infusion fluid, both high-calorie fluid and crystalloid fluid were included in the study.

Patients and methods

A retrospective review of medical records from the 12 hospitals was conducted. CD patients who underwent initial intestinal surgery (bowel resection, strictureplasty, and/or stoma construction) at any of the 12 hospitals between January 1970 and December 2009 were collected ($n = 1{,}703$). Of the 1,703 patients, patients who developed IF by December 2010 were reviewed ($n = 68$), and the cumulative risk for developing IF after initial intestinal surgery was evaluated. In addition, CD patients with IF who underwent initial intestinal surgery at other hospitals and were then treated at any of the 12 hospitals were also reviewed ($n = 41$). Of the 41 patients, eight were excluded

Table 1 Number of CD/IF patients who underwent initial intestinal surgery at the 12 participating hospitals by decade

	Time of initial intestinal surgery				
	1970–1979	1980–1989	1990–1999	2000–2009	Total
CD patients	37	139	511	1,016	1,703
CD patients with IF	2 (5.4 %)	12 (8.6 %)	33 (6.5 %)	21 (2.1 %)	68 (4.0 %)

CD Crohn's disease, *IF* intestinal failure

from the present study because of insufficient clinical data. Hence, a total of 101 CD patients with IF were collected, and their characteristics were reviewed. The cumulative risk for IF-related death by the time from the occurrence of IF was evaluated.

The following clinical data were collected in patients with IF: age at diagnosis of CD, age at initial intestinal surgery, age at the occurrence of IF, age at the time of the study, number of surgeries to the occurrence of IF, bowel disease location, length of remnant small intestine at the occurrence of IF (which was evaluated by the findings at the surgery), medical therapies, and complications after the occurrence of IF.

Statistical analysis

The cumulative risks of IF after initial intestinal surgery and IF-related death by the time from the occurrence of IF were evaluated using the Kaplan–Meier method. CD patients without IF were regarded as censored cases. Quantitative and qualitative variables were compared using the Mann–Whitney U test. Values of $P < 0.05$ were considered significant. All statistical analyses were performed using SPSS® version 13.0J software (SPSS Japan, Tokyo, Japan).

Results

Cumulative risk of IF

A total of 1,703 CD patients underwent initial intestinal surgery at any of the 12 hospitals between 1970 and 2009 (Table 1). Of the 1,703 patients, 68 (4.0 %) developed IF. The cumulative risk for developing IF after the initial intestinal surgery was 0.8 % (5 years), 3.6 % (10 years), 6.1 % (15 years), and 8.5 % (20 years) (Fig. 1a).

In consideration of the historical bias, the cumulative risk of IF was also evaluated excluding 176 patients who underwent initial surgery between 1970 and 1989. A total of 1,527 CD patients underwent initial intestinal surgery at any of the 12 hospitals between 1990 and 2009. Of the 1,527 patients, 54 (3.5 %) developed IF. The cumulative risk of IF after the initial intestinal surgery was 0.6 % (5 years), 2.8 % (10 years), and 4.9 % (15 years) (Fig. 1b).

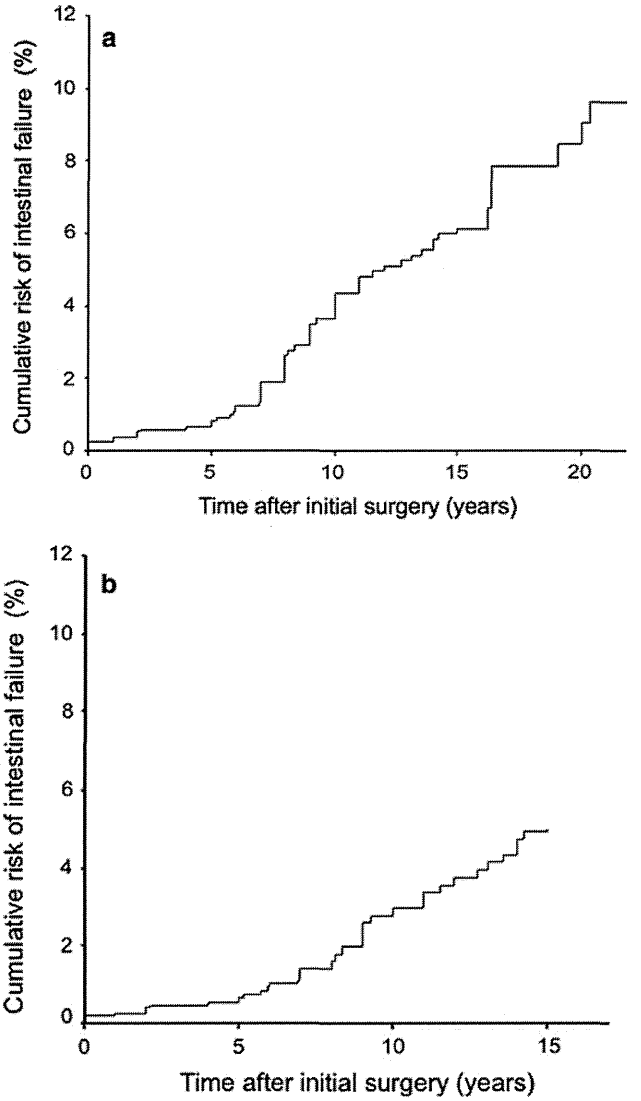

Fig. 1 Kaplan–Meier curve for the cumulative risk of intestinal failure in CD patients who underwent initial surgery between 1970 and 2009 (n = 1,703) (**a**) and between 1990 and 2009 (n = 1,527) (**b**)

Characteristics of CD patients with IF

The characteristics of the 101 CD patients with IF are shown in Table 2. The mean duration between CD diagnosis and the initial intestinal surgery was 6.4 years, and the mean duration between the initial surgery and the

Table 2 The characteristics of CD patients with IF ($n = 101$)

Age at (years)	
Diagnosis of CD	21.8 ± 8.8
Initial intestinal surgery	28.2 ± 9.3
Occurrence of IF	38.2 ± 10.7
Present (or age at death)	46.1 ± 11.4
No. of intestinal surgeries (times)	3.3 ± 1.7
Length of the small bowel (cm)	162 ± 64
Stoma	
Present (jejuno- or ileostomy/colostomy)	65 cases (64 %) (45/40)
Absent	36 (36 %)
Ileocecal valve	
Preserved	15 (15 %)
Resected	86 (85 %)

Mean ± SD

CD Crohn's disease, *IF* intestinal failure

Table 3 The characteristics of CD patients with IF who underwent initial surgery between 1990 and 2009 ($n = 63$)

Age at (years)	
Diagnosis of CD	21.1 ± 7.9
Initial intestinal surgery	29.1 ± 7.9
Occurrence of IF	35.8 ± 8.9
Present (or age at death)	42.0 ± 9.1
No. of intestinal surgeries (times)	3.1 ± 1.8
Length of the small bowel (cm)	176 ± 65
Stoma	
Present (jejuno- or ileostomy/colostomy)	46 cases (73 %) (36/10)
Absent	17 (27 %)
Ileocecal valve	
Preserved	8 (13 %)
Resected	55 (87 %)

Mean ± SD

CD Crohn's disease, *IF* intestinal failure

occurrence of IF was 10.0 years. The mean number of intestinal surgeries to the occurrence of IF was 3.3, and the mean length of remnant small intestine at the time of IF was 162 cm. The mean duration of follow-up after the occurrence of IF was 7.9 years. Sixty-five patients (64 %) had a stoma (jejuno- or ileostomy, $n = 45$; colostomy, $n = 20$), and 86 patients (86 %) had a resected ileocecal valve at the time of IF occurrence.

The characteristics of the 63 CD patients with IF who underwent initial surgery between 1990 and 2009 are shown in Table 3. Comparing the 38 CD patients with IF who underwent initial surgery before 1990, the mean length of remnant small intestine was significantly longer (176 vs. 138 cm, $P = 0.002$) and more patients had a stoma (73 vs. 50 %, $P = 0.022$).

Table 4 Medical treatments for CD patients with IF ($n = 101$)

	Before IF	After IF
HPN alone	–	4 cases (4 %)
5-ASA or sulphasalazine	76 cases (75 %)	74 (73 %)
Enteral nutrition	68 (67 %)	62 (61 %)
Steroid	48 (48 %)	28 (28 %)
Antimicrobial agent	29 (29 %)	31 (31 %)
Anti-TNF therapy	11 (11 %)	30 (30 %)
Immune-regulating agent	9 (9 %)	21 (21 %)
Cytapheresis	1 (1 %)	2 (2 %)
Intestinal surgery	101 cases	20 (20 %)
Unknown	11 cases	2 cases

CD Crohn's disease, *IF* intestinal failure, *HPN* home parenteral nutrition, *5-ASA* 5-aminosalicylic acid

Table 5 Medical treatments for CD patients with IF who underwent initial surgery between 1990 and 2009 ($n = 63$)

	Before IF	After IF
HPN alone	–	2 cases (3 %)
5-ASA or sulphasalazine	51 cases (81 %)	51 (81 %)
Enteral nutrition	44 (70 %)	41 (65 %)
Steroid	33 (52 %)	22 (35 %)
Antimicrobial agent	20 (32 %)	23 (37 %)
Anti-TNF therapy	7 (11 %)	21 (33 %)
Immune-regulating agent	5 (8 %)	12 (19 %)
Cytapheresis	1 (2 %)	1 (2 %)
Intestinal surgery	63 cases	13 (21 %)
Unknown	5 cases	1 cases

CD Crohn's disease, *IF* intestinal failure, *HPN* home parenteral nutrition, *5-ASA* 5-aminosalicylic acid

Medical treatments

The medical treatments for the CD patients with IF are shown in Table 4. Enteral nutrition was used in 68 patients (67 %) before the occurrence of IF and 62 patients (61 %) after the occurrence of IF. Twenty patients (20 %) underwent intestinal surgery during the mean 7.9 years of follow-up after the occurrence of IF. No patient underwent small bowel transplantation. The medical treatments for the CD patients with IF who underwent initial surgery between 1990 and 2009 are shown in Table 5. There were no significant differences in terms of medical treatment comparing the CD patients with IF who underwent initial surgery before 1990.

The intravenous infusion therapy given to the CD patients with IF is shown in Table 6. Excluding cases who died ($n = 12$) and weaned-off cases ($n = 16$), 73 IF

Table 6 Intravenous infusion therapy for CD patients with IF ($n = 73$)

Frequency of infusion (per week)	
7 times	58 cases (78 %)
4–6 times	4 (5 %)
3.5 times	7 (10 %)
2–3 times	4 (5 %)
Volume of infusion (per one time, mL)	
<1000	6 (8 %)
1000–2000	37 (51 %)
2000–3000	24 (33 %)
≥3000	6 (8 %)
Type of infusion	
High-calorie infusion	70 (96 %)
Crystalloid infusion	3 (4 %)

Excluding cases who died ($n = 12$) and weaned-off cases ($n = 16$), 73 IF patients were reviewed

patients were reviewed. Sixty-nine patients (95 %) used intravenous infusion therapy at least every second day, and 58 patients (79 %) used intravenous infusion every day. The median volume of infusion per time was 1500 mL. Seventy patients (96 %) used high-calorie infusion. The median number of calories by infusion was 1160 kcal/day.

Complications

Complications after the occurrence of IF are shown in Table 7. Seventy-nine patients (78 %) had at least one complication during the mean 7.9 years of follow-up after the occurrence of IF. Central venous catheter-related bloodstream infection (CRBSI) was the most frequent complication ($n = 58$, 57 %). Of the 58 patients, four died due to CRBSIs (Table 8). The frequency of CRBSI in CRBSI-related death cases ($n = 4$) was 2.4 times per 1000 days (mean), which was not significantly different from the other CRBSI cases ($n = 54$; 1.8 times per 1000 days) ($P = 0.636$). Liver dysfunction was the second most frequent complication ($n = 32$, 32 %).

Outcomes

The outcomes of CD patients with IF are shown in Table 8. Twelve patients (12 %) had died at 7.0 ± 4.0 years (mean ± SD) of follow-up after the occurrence of IF. The durations from the occurrence of IF to death were 4.5 ± 2.4 years (CRBSI), 7.4 ± 5.2 years (anorectal cancer), and 10.9 ± 4.5 years (liver cirrhosis). The ages at death were 37.5 ± 8.5 years (CRBSI), 59.4 ± 14.7 years (anorectal cancer), and 59.7 ± 14.6 years (liver cirrhosis). The cumulative risk of IF-related death (CRBSI or liver cirrhosis; $n = 6$) by the time from the occurrence of IF was 1.1 % (3 years), 3.7 % (5 years), 6.5 % (7 years), and 8.9 % (10 years) (Fig. 2). Sixteen patients (16 %) were weaned from IF status after 4.1 ± 2.1 years from the occurrence of IF.

Table 7 Complications after the occurrence of IF ($n = 101$)

Complications			
Yes	79 cases (78 %)		
No	16 (16 %)		
Unknown	6 (6 %)		
CV catheter-related complication		Metabolic complication	
CRBSI	58 cases (57 %)	Liver dysfunction	32 cases (32 %)
Catheter obstruction	16 (16 %)	Mineral deficiency/excess	14 (14 %)
Loss of venous access	7 (7 %)	Vitamin B12 deficiency	12 (12 %)
Skin trouble at CV port	6 (6 %)	Renal dysfunction	12 (12 %)
CV port broken	4 (4 %)	Dehydration	11 (11 %)
Subcutaneous infection	3 (3 %)	Gall bladder stone	6 (6 %)
Infection		Renal stone	5 (5 %)
Infective endocarditis	2 (2 %)	Hyperuricemia	2 (2 %)
Fungal endophthalmitis	1 (1 %)	Electrolyte abnormality	2 (2 %)
Cerebral meningitis	1 (1 %)	Amyloidosis	1 (1 %)
Brain abscess	1 (1 %)	Growth disorder	1 (1 %)
Splenic abscess	1 (1 %)	Osteoporosis	1 (1 %)
Others		Renal anemia	1 (1 %)
Skin trouble	4 (4 %)		
Thrombosis	3 (3 %)		
GI hemorrhage	3 (3 %)		
Depression	2 (2 %)		

IF intestinal failure, *CV* central venous, *CRBSI* catheter-related bloodstream infection, *GI* gastrointestinal

Discussion

The present study showed that the cumulative risk of IF in CD patients, who underwent initial intestinal surgery between 1970 and 2009, was less than 1 % at 5 years after the initial surgery, but the risk increased over 5 % at 15 years after the initial surgery. Because medical treatments and surgical techniques have changed, the authors also evaluated the risk of IF excluding patients who underwent initial surgery between 1970 and 1989 to avoid the historical bias. The cumulative risk of IF was still nearly 5 % at 15 years after the initial surgery. To the best of our

Table 8 Prognosis of CD patients with IF ($n = 101$)

Deaths	12 cases (12 %)
CRBSI	4 (4 %)
Anorectal cancer	4 (4 %)
Liver cirrhosis	2 (2 %)
Suicide	1 (1 %)
Intestinal perforation	1 (1 %)
Weaned off cases	16 (16 %)

CD Crohn's disease, *IF* intestinal failure, *CRBSI* catheter-related bloodstream infection

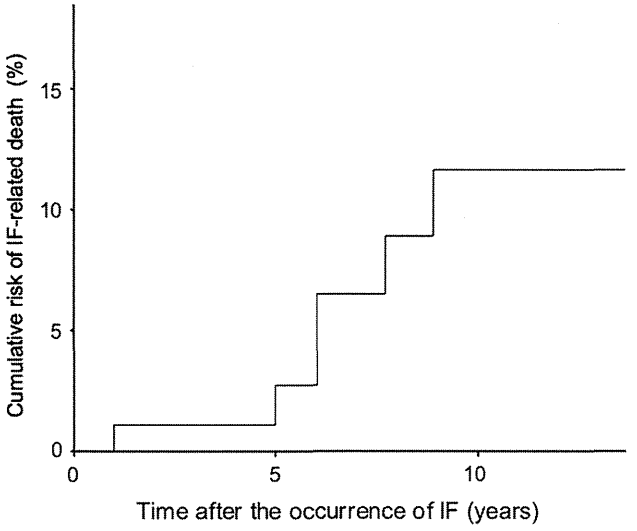

Fig. 2 Kaplan–Meier curve for the cumulative risk of IF-related death in CD patients with IF ($n = 101$)

knowledge, the present study is the first to estimate the cumulative risk for developing IF in patients with CD using the Kaplan–Meier method. To date, there has been a very limited number of studies concerning the incidence of IF in patients with CD. Most of these studies were population-based studies or small-sized studies, and they only assessed the incidence of IF at one time point [11–15]. Hurst et al. [13] reported that four (0.8 %) of 513 CD patients who underwent surgery between 1985 and 1996 developed IF, which was a short-term result, because the study was published in 1997. Dietz et al. [14] reported that 23 (10 %) of 219 CD patients developed IF at a median follow-up of 7.8 years after the initial operation. Yamamoto et al. [15] reported that two (4.5 %) of 44 CD patients developed IF at a median follow-up of 15 years after the initial operation. These studies support the present results; the occurrence of IF in CD patients is rare in the short-term period after initial surgery, though it is not rare over the long term.

In the present study, the term "intestinal failure (IF)" was used instead of the term "short bowel syndrome (SBS)" because the term "SBS" seems to indicate that the degree of malabsorption only depends on the length of the residual bowel itself [16]. However, both intestinal length and intestinal function affect the severity of malabsorption [17]. The term "IF" is a more general expression and refers directly to the intestinal function itself [16]. In CD patients, the intestinal absorptive function may be affected by the disease activity, as well as the bowel length; therefore, the present study used the term "IF" from the clinical standpoint. From the standpoint of intestinal length, in the present study, the mean length of remnant small intestine was 162 cm. The American Gastroenterological Association Clinical Practice Committee stated that SBS can occur when there is less than 200 cm of small bowel [10]. Hurst et al. [13] noted that 5 % of patients with CD were left with intestinal remnants of less than 180 cm after multiple resections, and were at risk for the development of SBS. These findings were consistent with the present study.

The present study showed that death was not rare in CD patients with IF. Several studies have reported that the overall 5-year mortality in HPN-treated patients (including CD and other diseases) ranged from 2 to 28 %, though most of these studies were population-based studies, and the precise mortality of CD patients with IF was still unclear [18–21]. To the best of our knowledge, the present study is the first to have estimated IF-related death in CD patients using the Kaplan–Meier method. The poor prognosis was mainly due to complications of HPN (CRBSI, liver dysfunction) and anorectal cancer. Since CRBSI and liver dysfunction were the most frequent complications in CD patients with IF, it is very important to prevent and/or manage these complications. In terms of CRBSI, previous studies reported that the occurrence rate of CRBSI in HPN patients (including CD and other diseases) ranged from 0.44 to 3 times per 1000 days [22–24]. The Center for Disease Control and Prevention (CDC) guideline recommended the use of a prophylactic antimicrobial lock solution in patients with long-term catheters who have a history of multiple CRBSIs despite optimal maximal adherence to aseptic technique [25]. In terms of liver dysfunction, parenteral nutrition–induced liver disease varies from steatosis due to excessive caloric administration to severe cholestatic injury with irreversible cirrhosis [26]. Optimal methods for preventing or retarding the development of liver dysfunction have not been established, although several have been proposed. A few recent studies indicated that substituting fish oil-based lipid solutions (rich in omega-3 fatty acids) may improve parenteral nutrition-associated cholestasis [27, 28]. Intestinal and/or liver transplantation is an option for some patients for whom other treatments have failed and who have complications from long-term parenteral nutrition. These patients are typically considered for transplantation as a result of the loss of venous access sites, recurrent and

persistent episodes of sepsis, and development of liver failure.

Finally, the limitations of the present study must be considered. Because the present study is a long-term study, there is a bias in terms of medical treatments. Recent studies showed that anti-TNF therapy was effective in maintaining remission in Crohn's disease [29, 30]and reduced the rate of surgery [31]. Another recent study showed that teduglutide, a glucagon-like peptide-2 (GLP-2) analogue, reduced volumes and numbers of days of parenteral support for SBS patients with IF (including CD and other diseases) [32]. There is a possibility that recent medical treatments including anti-TNF therapy and teduglutide reduce the occurrence of IF and/or prompts weaning from IF status in CD patients, though another long-term study is essential to clarify the issue. Similar to medical therapy, factors such as materials (e.g., central venous catheter) and infection countermeasures have changed over time. These factors may improve the managements of the IF patients and may reduce late complications, though further study is also needed to clarify the issue.

In conclusion, the present study showed that the incidence of IF in CD patients was not low over the long-term after initial surgery. CRBSI and liver dysfunction were the most frequent complications, and the poor prognosis was mainly due to these complications. To date, there are few treatments for SBS patients with IF [33]. There is a pressing need to develop strategies for the prevention and management of IF.

Acknowledgments The authors thank Hitoshi Ogawa and Sho Haneda (Tohoku University Hospital), Ken-ichi Takahashi (Tohoku Rosai Hospital), Daijiro Higashi (Fukuoka University Chikushi Hospital), Michio Itabashi and Shinpei Ogawa (Tokyo Women's Medical University), Toshimitsu Araki (Mie University Hospital), Keiji Matsuda (Teikyo University Hospital), Shinji Nakamura (Nara Medical University Hospital), Katsuyoshi Hatakeyama and Tsuneo Iiai (Nigata University Hospital), and Masahiko Watanabe (Kitasato University Hospital) for collecting data and/or important intellectual contributions.

Conflict of interest This work was supported in part by Health and Labour Sciences Research Grants for research on intractable diseases from the Ministry of Health, Labour and Welfare of Japan.

References

1. Vernier-Massouille G, Balde M, Salleron J, et al. Natural history of pediatric Crohn's disease: a population-based cohort study. Gastroenterology. 2008;135:1106–13.
2. Bernell O, Lapidus A, Hellers G. Risk factors for surgery and recurrence in 907 patients with primary ileocaecal Crohn's disease. Br J Surg. 2000;87:1697–701.
3. Bernell O, Lapidus A, Hellers G. Risk factors for surgery and postoperative recurrence in Crohn's disease. Ann Surg. 2000;231:38–45.
4. Basilisco G, Campanini M, Cesana B, et al. Risk factors for first operation in Crohn's disease. Am J Gastroenterol. 1989;84:749–52.
5. Peyrin-Biroulet L, Loftus EV Jr, Colombel JF, et al. The natural history of adult Crohn's disease in population-based cohorts. Am J Gastroenterol. 2010;105:289–97.
6. Williams J, Wong W, Rothenberger D, et al. Recurrence of Crohn's disease after resection. Br J Surg. 1991;78:10–9.
7. Greenstein AJ, Sachar DB, Pasternack BS, et al. Reoperation and recurrence in Crohn's colitis and ileocolitis Crude and cumulative rates. N Engl J Med. 1975;293:685–90.
8. Fleming CR, Remington M. Intestinal failure. In: Hill GI, editor. Nutrition and the surgical patients. Clinical Surgery International. Edinburgh: Churchill Livingstone; 1981. p. 219–35.
9. Lal S, Teubner A, Shaffer JL. Review article: intestinal failure. Aliment Pharmacol Ther. 2006;24:19–31.
10. O'Keefe SJ, Buchman AL, Fishbein TM, et al. Short bowel syndrome and intestinal failure: consensus definitions and overview. Clin Gastroenterol Hepatol. 2006;4:6–10.
11. Mughal M, Irving M. Home parenteral nutrition in the United Kingdom and Ireland. Lancet. 1986;2:383–7.
12. Bakker H, Bozzetti F, Staun M, et al. Home parenteral nutrition in adults: a european multicentre survey in 1997. ESPEN-Home Artificial Nutrition Working Group. Clin Nutr. 1999;18:135–40.
13. Hurst RD, Molinari M, Chung TP, et al. Prospective study of the features, indications, and surgical treatment in 513 consecutive patients affected by Crohn's disease. Surgery. 1997;122:661–7.
14. Dietz DW, Fazio VW, Laureti S, et al. Strictureplasty in diffuse Crohn's jejunoileitis: safe and durable. Dis Colon Rectum. 2002;45:764–70.
15. Yamamoto T, Allan RN, Keighley MR. Long-term outcome of surgical management for diffuse jejunoileal Crohn's disease. Surgery. 2001;129:96–102.
16. Nordgaard I, Hansen BS, Mortensen PB. Importance of colonic support for energy absorption as small-bowel failure proceeds. Am J Clin Nutr. 1996;64:222–31.
17. Buchman AL, Scolapio J, Fryer J. AGA technical review on short bowel syndrome and intestinal transplantation. Gastroenterology. 2003;124:1111–34.
18. Messing B, Landais P, Goldfarb B, et al. Home parenteral nutrition for adults. Results of a multicenter survey in France. Presse Med. 1988;17:845–9.
19. Howard L, Ament M, Fleming CR, et al. Current use and clinical outcome of home parenteral and enteral nutrition therapies in the United States. Gastroenterology. 1995;109:355–65.
20. Silverberg MS, Satsangi J, Ahmad T, et al. Toward an integrated clinical, molecular and serological classification of inflammatory bowel disease: Report of a Working Party of the 2005 Montreal World Congress of Gastroenterology. Can J Gastroenterol. 2005;19 Suppl A:5–36.
21. Elriz K, Palascak-Juif V, Joly F, et al. Crohn's disease patients with chronic intestinal failure receiving long-term parenteral nutrition: a cross-national adult study. Aliment Pharmacol Ther. 2011;34:931–40.
22. Crispin A, Thul P, Arnold D, et al. Central venous catheter complications during home parenteral nutrition: a prospective pilot study of 481 patients with more than 30,000 catheter days. Onkologie. 2008;31:605–9.
23. Ireton-Jones C, DeLegge M. Home parenteral nutrition registry: a five-year retrospective evaluation of outcomes of patients receiving home parenteral nutrition support. Nutrition. 2005;21:156–60.
24. Reimund JM, Arondel Y, Finck G, et al. Catheter-related infection in patients on home parenteral nutrition: results of a prospective survey. Clin Nutr. 2002;21:33–8.
25. O'Grady NP, Alexander M, Burns LA, et al. Guidelines for the prevention of intravascular catheter-related infections. Am J Infect Control. 2011;39(Suppl 1):S1–34.

26. Vanderhoof JA, Langnas AN. Short-bowel syndrome in children and adults. Gastroenterology. 1997;113:1767–78.
27. Gura KM, Duggan CP, Collier SB, et al. Reversal of parenteral nutrition-associated liver disease in two infants with short bowel syndrome using parenteral fish oil: implications for future management. Pediatrics. 2006;118:197–201.
28. Gura KM, Lee S, Valim C, et al. Safety and efficacy of a fish-oil-based fat emulsion in the treatment of parenteral nutrition-associated liver disease. Pediatrics. 2008;121:678–86.
29. Yoshida K, Fukunaga K, Ikeuchi H, et al. Scheduled infliximab monotherapy to prevent recurrence of Crohn's disease following ileocolic or ileal resection: a 3-year prospective randomized open trial. Inflamm Bowel Dis. 2012;18:1617–23.
30. Colombel JF, Sandborn WJ, Reinisch W, et al. Infliximab, azathioprine, or combination therapy for Crohn's disease. N Engl J Med. 2010;362:1383–95.
31. Lichtenstein GR, Yan S, Bala M, et al. Infliximab maintenance treatment reduces hospitalizations, surgeries, and procedures in fistulizing Crohn's disease. Gastroenterology. 2005;128:862–9.
32. Jeppesen PB, Pertkiewicz M, Messing B, et al. Teduglutide reduces need for parenteral support among patients with short bowel syndrome with intestinal failure. Gastroenterology. 2012; 143:1473–81.
33. Buchman AL. Teduglutide and short bowel syndrome: every night without parenteral fluids is a good night. Gastroenterology. 2012;143:1416–20.